Optimizing sampling strategies in high-resolution paleoclimate records

Niels J. de Winter[1,2] *, Tobias Agterhuis[1], Martin Ziegler[1]

[1]Department of Earth Sciences, Utrecht University, Princetonlaan 8a, 3584 CB Utrecht, the Netherlands

[2]AMGC research group, Vrije Universiteit Brussel, Pleinlaan 2, 1050 Brussels, Belgium

Correspondence to: Niels J. de Winter (n.j.dewinter@uu.nl)

When calling out to supp figs, please use, e.g. "Fig. S2" not just "S2"

Abstract

The aim of paleoclimate studies to resolve climate variability from noisy proxy records can in essence be reduced to a statistical problem. The challenge is to extract meaningful information about climate variability from these records by reducing measurement uncertainty through a combination of proxy data while retaining the temporal resolution needed to assess the timing and duration of variations in climate parameters. In this study, we explore the limits of this compromise by testing different methods for combining proxy data (smoothing, binning and sample size optimization) on a particularly challenging paleoclimate problem: resolving seasonal variability in stable isotope records. We test and evaluate the effects of changes in the seasonal temperature and the hydrological cycle as well as changes in accretion rate of the archive and parameters such as sampling resolution and age model uncertainty on the reliability of seasonality reconstructions based on clumped and oxygen isotope analyses in 33 real and virtual datasets. Our results show that strategic combinations of clumped isotope analyses can significantly improve the accuracy of seasonality reconstructions compared to conventional stable oxygen isotope analyses, especially in settings where the isotopic composition of the water is poorly constrained. Smoothing data using a moving average often leads to an apparent dampening of the seasonal cycle, significantly reducing the accuracy of reconstructions. A statistical sample size optimization protocol yields more precise results than smoothing. However, the most accurate results are obtained through monthly binning of proxy data, especially in cases where growth rate or water composition cycles obscure the seasonal temperature cycle. Our analysis of a wide range of natural situations reveals that the effect of temperature seasonality on oxygen isotope records almost invariably exceeds that of changes in water composition. Thus, in most cases, oxygen isotope records allow reliable identification of growth seasonality as a basis for age modelling in absence of independent chronological markers in the record. These specific findings allow us to formulate general recommendations for sampling and combining data in paleoclimate research and have implications beyond the reconstruction of seasonality. We briefly discuss the implications of our results for solving common problems in paleoclimatology and stratigraphy.

1. Introduction

is it worth adding some text here to provide context on the issue of age model uncertainty, which you tackle later?

Improving the resolution of climate reconstructions is a key objective in paleoclimate studies because it allows climate variability to be studied on different timescales and sheds light on the continuum of climate variability (Huybers and Curry, 2006). However, the temporal resolution of climate records is limited by the accretion rate (growth or sedimentation rate) of the archive and the spatial resolution of sampling for climate reconstructions, which is a function of the sample size required for a given climate proxy. This tradeoff between sample size and sampling resolution is especially prevalent when using state-of-the-art climate proxies which require large sample sizes, such as the carbonate clumped isotope paleothermometer (Δ_{47}; see applications in Rodríguez-Sanz et al., 2017; Briard et al., 2020; Caldarescu et al., 2021) or stable isotope ratios in specific compounds or of rare isotopes (e.g. phosphate-oxygen isotopes in tooth apatite, triple oxygen isotopes in speleothems or carbon isotopes of CO_2 in ice cores; Jones et al., 1999; Schmitt et al., 2012; Sha et al., 2020). The challenge of sampling resolution persists on a wide range of timescales: from attempts to resolve geologically short-lived (kyr-scale) climate events from deep sea cores with low sedimentation rates (e.g. Stap et al., 2010; Rodríguez-Sanz et al., 2017) to efforts to characterize tidal or daily variability in accretionary carbonate archives (e.g. Warter and Müller, 2017; de Winter et al., 2020a). What constitutes “high-resolution” is therefore largely dependent on the specifics of the climate archive.

Sample size limitations are especially important in paleoseasonality reconstructions. Reliable archives for seasonality (e.g. corals, mollusks and speleothem records) are in high demand in the paleoclimate community, because the seasonal cycle is one of the most important cycles in Earth’s climate and seasonality reconstructions complement more common long-term (kyr to -Myr) records of past climate variability (e.g. Morgan and van Ommen, 1997; Tudhope et al., 2001; Steuber et al., 2005; Steffensen et al., 2008; Denton et al., 2005; Huyghe et al., 2015; Vansteenberge et al., 2019). A more detailed understanding of climate dynamics at the human timescale is increasingly relevant for improving climate projections (IPCC, 2013). Unfortunately, the growth and mineralization rates of archives that capture high-resolution variability (rarely exceeding 10 mm/yr) limit the number and size of samples that can be obtained at high temporal resolutions (e.g. Mosley-Thompson et al., 1993; Passey and Cerling, 2002; Treble et al., 2003; Goodwin et al., 2003). This problem is exacerbated by the fact that accurate methods for climate

reconstructions often require comparatively large sample sizes while methods relying on smaller sample sizes rely on uncertain assumptions. A case in point is the popular carbonate stable oxygen isotope temperature proxy ($\delta^{18}O_c$) which relies on assumptions of the water composition ($\delta^{18}O_w$) that become progressively more uncertain further back in geological history (e.g. Veizer and Prokoph, 2015). Contrarily, the clumped isotope proxy (Δ_{47}) does not rely on this assumption but requires larger amounts of sample (e.g. Müller et al., 2017)

A promising technique for circumventing sample size limitations is to analyze larger numbers of small aliquots from the same sample or from similar parts of the climate archive. These smaller aliquots typically have poor precision but averaging multiple aliquots into one estimate while propagating the measurement uncertainty leads to a more reliable estimate of the climate variable (Dattalo, 2008; Meckler et al., 2014; Müller et al., 2017; Fernandez et al., 2017). This approach yields improved sampling flexibility since aliquots can be combined in various ways after measurement. It also allows outlier detection at the level of individual aliquots, thereby spreading the risk of instrumental failure and providing improved control on changes in measurement conditions that may bias results.

Previous studies have applied several different methods for combining data from paleoclimate records to reduce analytical noise or higher order variability, and extract variability with a specific frequency (e.g. a specific orbital cycle or seasonality; e.g. Lisiecki and Raymo, 2004; Cramer et al., 2009). These data reduction approaches can in general be categorized into **smoothing** techniques, in which a sliding window or range of neighboring datapoints is used to smooth high resolution records (see e.g. Cramer et al., 2009) or **binning** techniques, in which the record is divided into equal bins in sampling direction (e.g. time, depth or length in growth direction; e.g. Lisiecki and Raymo, 2004; Rodríguez-Sanz et al., 2017). In addition, a third approach is proposed here based on **optimization** of sample size for dynamic binning of data along the climate cycle using a moving window in the domain of the climate variable (as opposed to the sampling domain) combined with a T-test routine (see section **2.1**). All three approaches have advantages and caveats.

In this study, we explore the (dis)advantages of these three data reduction approaches by testing their reliability in resolving seasonal variability in sea surface temperature (SST) and water stable oxygen isotope

composition ($\delta^{18}O_w$), both highly sought-after variables in paleoclimate research. We compare reconstructions of SST and $\delta^{18}O_w$ in real and virtual datasets from accretionary carbonate archives (e.g. shells, corals and speleothems) using the clumped isotope thermometer (Δ_{47}) combined with stable oxygen isotope ratios of the carbonate ($\delta^{18}O_c$).

2. Methods

2.1 Reconstruction approaches

Throughout the remainder of this work, the three approaches for combining data for reconstructions are defined as follows (see also **Fig. 1**):

Smoothing refers to the reconstruction of SST and $\delta^{18}O_w$ based on **moving averages** of Δ_{47} and $\delta^{18}O_c$ records (**Fig. 1B**). For every dataset, the full possible range of moving window sizes (from 1 sample to the full length of the record) for SST and $\delta^{18}O_w$ reconstructions was explored. The window size that resulted in the most significant difference between maximum and minimum Δ_{47} values (based on a student's T-test) was applied to reconstruct SST and $\delta^{18}O_w$ from Δ_{47} and $\delta^{18}O_c$ records. SST and $\delta^{18}O_w$ were calculated for all case studies using a combination of empirical temperature relationships by Kim and O'Neil (1997; $\delta^{18}O_c$-$\delta^{18}O_w$-temperature relationship) and Bernasconi et al. (2018; Δ_{47}-temperature relationship). Here and in other approaches, a typical analytical uncertainty on measurements of Δ_{47} (one standard deviation of 0.04‰) and $\delta^{18}O_c$ (one standard deviation of 0.05‰) was used to include uncertainty due to measurement precision. These analytical uncertainties were chosen based on typical uncertainties reported for these measurements in the literature (e.g. Schöne et al., 2005; Huyghe et al., 2015; Vansteenberge et al., 2016) and long-term precision uncertainties obtained by measuring in-house standards using the MAT253+ with Kiel IV setup in the clumped isotope laboratory at Utrecht University (e.g. Kocken et al., 2019). The measurement uncertainty was propagated through all calculations using a Monte Carlo simulation (N = 1000) in which Δ_{47} and $\delta^{18}O_c$ records were randomly sampled from a normal distribution with the virtual Δ_{47} and $\delta^{18}O_c$ values as means and analytical uncertainties as standard deviations.

Binning refers to reconstructions of SST and $\delta^{18}O_w$ based on binning of Δ_{47} and $\delta^{18}O_c$ records into monthly time bins (**Fig. 1C**). The Δ_{47} and $\delta^{18}O_c$ data from each case study were grouped into monthly time bins and converted to SST and $\delta^{18}O_w$ using the Kim and O'Neil (1997) and Bernasconi et al. (2018) formulae. Here too, Monte Carlo simulation was applied to propagate measurement uncertainties onto monthly SST and $\delta^{18}O_w$ reconstructions. Note that the prerequisite for this method is that the data is aligned using a (floating) age model accurate enough to allow samples to be placed in the right bin. The age of virtual samples in this study is known so this prerequisite poses no problems in this case. However, in the fossil record this alignment might be less certain in absence of accurate chronologies within the archive (e.g. through daily growth increments in mollusk shells; e.g. Schöne et al., 2008; Huyghe et al., 2019; see 4.1.3).

Optimization refers to reconstructions of SST and $\delta^{18}O_w$ based on sample size optimization in Δ_{47} records (**Fig. 1D**). In this approach aliquots of each virtual dataset are ordered from warm (low $\delta^{18}O_c$) to cold (high $\delta^{18}O_c$ data) samples, regardless of their position relative to the seasonal cycle. From this ordered dataset, increasingly large samples of multiple aliquots (from 2 aliquots to half the length of the record) are taken from both the warm ("summer") and the cold ("winter") side of the distribution. Summer and winter samples were kept equal (symmetrical grouping) to reduce the number of possible sample size combinations and allow for more efficient computation. However, asymmetrical grouping with differing sample sizes on the summer and winter ends of the $\delta^{18}O_c$-spectrum are possible (see 4.1.3 and 4.2.2). Sample sizes with significant difference in Δ_{47} value between summer and winter groups ($p \leq 0.05$ based on a student's T-test) were selected as optimal sample sizes. The moving window T-test in the proxy domain ensures that an optimal compromise is reached between high precision and resolving differences between seasonal extremes. For each successful sample size, SST and $\delta^{18}O_w$ values were calculated from Δ_{47} and $\delta^{18}O_c$ data according to Kim and O'Neil (1997) and Bernasconi et al. (2018) formulae. The relationship between SST and $\delta^{18}O_w$ obtained from these reconstructions was used to convert all Δ_{47} and $\delta^{18}O_c$ data to SST and $\delta^{18}O_w$, which are then grouped into monthly SST and $\delta^{18}O_w$ reconstructions. Measurement uncertainties were propagated through the entire approach by Monte Carlo simulation (N = 1000).

For comparison, we also include reconstructions based solely on $\delta^{18}O_c$ measurements with an (often inaccurate) assumption of a constant $\delta^{18}O_w$ (equal to the modern ocean value of 0‰ VSMOW), which form

the most common method for carbonate-based temperature reconstructions in paleoclimate research (see e.g. Schöne et al., 2005; Westerhold et al., 2020; **Fig. 1A**; hereafter: **$\delta^{18}O$**). For these reconstructions, $\delta^{18}O_c$ records were grouped into monthly time bins with analytical uncertainties propagated using the Monte Carlo approach (N = 1000) and were directly converted to SST using the Kim and O'Neil (1997) temperature relationship.

For each reconstruction, SST and $\delta^{18}O_w$ results were aggregated into monthly averages, medians, standard deviations, and standard errors. Step by step documentation of calculations made for the three Δ_{47}-based reconstruction approaches and the $\delta^{18}O_c$ reconstructions are given in **S7** and in the complementary R package (de Winter, 2021a).

2.2 Benchmarks for accuracy and precision

Accuracy and precision of reconstructions were evaluated against official USGS definitions of climate parameters (O'Donnell et al., 2012):

1. mean annual SST (MAT), defined as the average of all 12 monthly temperature reconstructions.
2. seasonal range in SST, defined as the temperature difference between warmest and coldest month.
3. mean annual $\delta^{18}O_w$, defined as the average of all 12 monthly $\delta^{18}O_w$ reconstructions.
4. seasonal range in $\delta^{18}O_w$, defined as the $\delta^{18}O_w$ difference between most enriched (highest $\delta^{18}O_w$) and most depleted (lowest $\delta^{18}O_w$) monthly reconstruction.

Accuracy was defined as the absolute offset of the reconstructed climate parameter from the "true" value. Precision was defined as the (relative) standard deviation of the reconstruction, as calculated from the variability within monthly time bins resulting from Monte Carlo error propagation (see **2.1**). An overview of monthly SST and $\delta^{18}O_w$ reconstructions using the four approaches in all cases is given in **S4**. Raw data and figures of reconstructions of all cases using all sampling resolutions are compiled in **S8**.

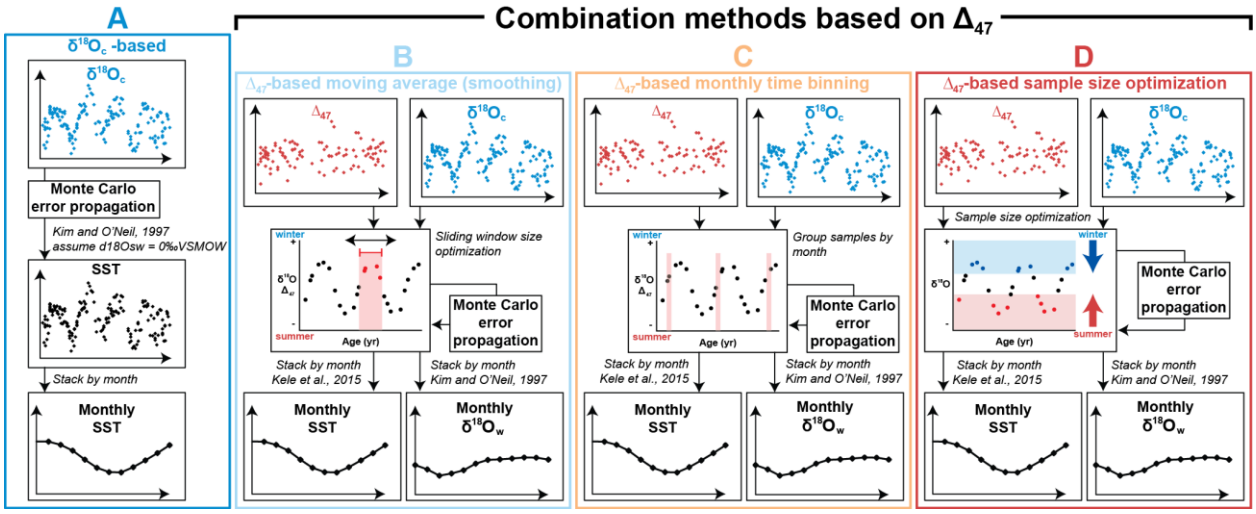

***Figure 1**: Schematic overview of the four approaches for seasonality reconstructions: (**A**) **$\delta^{18}O$**-based reconstructions, assuming constant $\delta^{18}O_w$. (**B**) Reconstructions based on **smoothing** $\delta^{18}O_c$ and Δ_{47} data using a moving average. (**C**) Reconstructions based on binning $\delta^{18}O_c$ and Δ_{47} data in monthly time bins. (**D**) Reconstructions based on **optimization** of the sample size for combining $\delta^{18}O_c$ and Δ_{47} data (see description in **2.1**). Colored curves represent virtual $\delta^{18}O_c$ (blue) and Δ_{47} (red) series in sampling domain. Black curves represent reconstructed monthly SST and $\delta^{18}O_w$ averages.*

2.3 SST and $\delta^{18}O_w$ datasets

The three reconstruction approaches were tested and compared based on three types of data: Firstly, data from a real specimen of a Pacific oyster (*Crassostrea gigas*, syn. *Magallana gigas*) reported in Ullmann et al. (2010). Secondly, data based on actual measurements of natural variability in SST and sea surface salinity (SSS; case 30-33) converted to virtual Δ_{47} and $\delta^{18}O_c$ records. Thirdly, a set of datasets based on fully artificial SST and $\delta^{18}O_w$ data (case 1-29; see **Fig. 2**) converted to virtual Δ_{47} and $\delta^{18}O_c$ records.

see notes in subsequent pages for idea for clearer nomenclature on these cases

→ Minor organizational point, but would be easier to follow if cases are presented consecutively, starting with cases 1-29, then 30-33, and finally the Pacific oyster (why not number this case 34?)

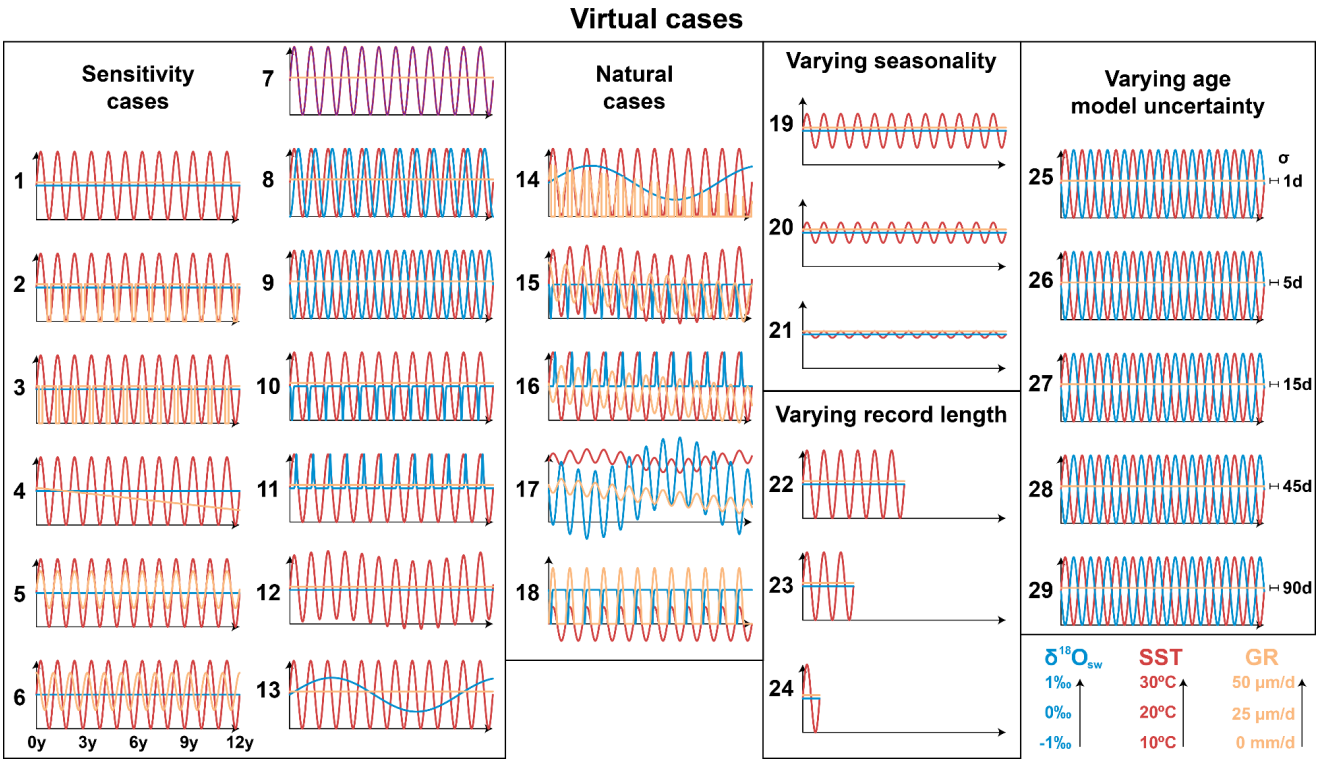

***Figure 2**: Overview of time series of all virtual test cases. Colored curves represent time series of SST (red), $\delta^{18}O_w$ (blue) and growth rate (orange, abbreviated as "GR"). Horizontal axes in all plots are 12 years long (see legend below case 6). Vertical axis of all plots has the same scale (SST: 10 to 30°C; $\delta^{18}O_w$: -1 to +1‰; Growth rate: 0 –50 µm/day; see legend in bottom right corner). Horizontal error bars and labels on the right side of cases 25-29 represent standard errors introduced on the age model (bars not to scale). The $\delta^{18}O_c$ and Δ_{47} records resulting from these virtual datasets are provided in **S6** (see also **Fig. 3** for natural examples).*

Sensitivity cases		Natural cases	Varying seasonality	Varying age model uncertainty
	7. $\delta^{18}O_w$ seasonality in phase with SST		**19.** Control case with reduced SST amplitude (~5°C)	
1. Control	**8.** $\delta^{18}O_w$ seasonality in antiphase with SST	**14.** Full marine case with ontogenetic GR trend	**20.** Control case with reduced SST amplitude (~3°C)	**25.** Case 9 with ±1 day age model uncertainty
2. Growth stops <12°C	**9.** $\delta^{18}O_w$ seasonality lags SST by ¼ year	**15.** Coastal case with spring $\delta^{18}O_w$ decrease and decreasing GR trend	**21.** Control case with reduced SST amplitude (~1°C)	**26.** Case 9 with ±5 days age model uncertainty
3. Growth stops >28°C	**10.** Negative $\delta^{18}O_w$ in spring	**16.** Lagoonal case with summer $\delta^{18}O_w$ increase	**Varying record length**	**27.** Case 9 with ±15 days age model uncertainty
4. Linear decrease in GR	**11.** Positive $\delta^{18}O_w$ in summer	**17.** Tropical monsoon case with confined SST seasonality and strong multi-annual SST cycle	**22.** Control case shortened to 6 yr	**28.** Case 9 with ±45 days age model uncertainty
5. GR seasonality in phase with SST	**12.** Multi-annual (5 yr) SST cycle	**18.** Worst-case scenario with growth limited to summer half of the year	**23.** Control case shortened to 3 yr	**29.** Case 9 with ±90 days age model uncertainty
6. GR seasonality lags SST by ¼ year	**13.** Multi-annual (5 yr) $\delta^{18}O_w$ cycle		**24.** Control case shortened to 1 yr	

Table 1*: Overview of virtual cases 1-29 used to test the reconstruction methods. Case descriptions are abbreviated. Details on the SST, growth rate and $\delta^{18}O_w$ included in each case are described in detail in* ***S1****. SST, growth rate and $\delta^{18}O_w$ records of all cases are shown in* ***Fig. 2****. "GR" = growth rate.*

2.3.1 Modern oyster data

Environmental SST and $\delta^{18}O_w$ data from the List Basin in Denmark (54°59.25N, 8°23.51E), where the modern oyster specimen lived, were obtained from local *in situ* measurements of SST and SSS described in Ullmann et al. (2010). Since direct, *in situ* measurements of $\delta^{18}O_w$ variability at a high temporal resolution were not available, $\delta^{18}O_w$ was estimated from more widely available SSS data using a mass balance (equation 1 and 2; following e.g. Ullmann et al., 2010):

$$\delta^{18}O_{sw} = \delta^{18}O_{w,freshwater} * f + \delta^{18}O_{w,ocean} * (1 - f) \qquad (1)$$

196 $$f = \frac{SSS_{sample} - SSS_{ocean}}{SSS_{freshwater} - SSS_{ocean}} \quad (2)$$

197 Here, we assume salinity (SSS_{sample}) results from a mixture of a fraction (*f*) isotopically light and low-salinity
198 ($\delta^{18}O_{w,freshwater}$ = -8.5‰; $SSS_{freshwater}$ = 0) freshwater and a fraction (*1-f*) ocean water ($\delta^{18}O_{w,ocean}$ = 0‰;
199 SSS_{ocean} = 35), with negative amounts of freshwater contribution (*f* < 0) representing net evaporation
200 ($SSS_{sample} > SSS_{ocean}$). The value for $\delta^{18}O_{w,freshwater}$ was based on the discharge weighted average $\delta^{18}O_w$ of
201 water in the nearby Elbe and Weser rivers (see Ullmann et al., 2010). All $\delta^{18}O_w$ values throughout the text
202 are with reference to the VSMOW scale. Contrary to the virtual datasets (cases 1-33; see **2.3.2** and **2.3.3**),
203 the Ullmann et al. (2010) data was already available in the sampling domain, hence no subsampling was
204 required.

205 *2.3.2 Cases based on real climate data* (measured environmental data; virtual/proxy data)

206 Four test cases were based on time series of real SST and SSS data from four different locations, selected
207 to capture a variety of environments with different SST and SSS variability (see **Fig. 3**):

208 1. Tidal flats of the Wadden Sea near Texel, the Netherlands (case 30)
209 2. Great Barrier Reef in Australia (case 31)
210 3. Gulf of Aqaba between Egypt and Saudi Arabia (case 32)
211 4. Northern Atlantic Ocean east of Iceland (case 33).

212 Daily measurements of SST and SSS for case 31-33 were obtained from worldwide open-access datasets
213 of the National Oceanic and Atmospheric Administration (NOAA, 2020) and European Space Agency (ESA,
214 2020) respectively. Hourly SST and SSS measured *in situ* in the Wadden Sea (case 30) were obtained
215 from the Dutch Institute for Sea Research (NIOZ, Texel, the Netherlands). Since direct, *in situ*
216 measurements of $\delta^{18}O_w$ variability at a high temporal resolution are scarce, $\delta^{18}O_w$ was estimated from (more
217 widely available) SSS data using the same mass balance described in **2.3.1**. The value for $\delta^{18}O_{w,freshwater}$
218 was based on the $\delta^{18}O_w$ of rain in the Netherlands (-8‰; Mook, 1970; Bowen, 2020). Applying this mass
219 balance on the SSS record of the Wadden Sea tidal flats (case 30) results in $\delta^{18}O_w$ values and a SSS-$\delta^{18}O_w$
220 relationship in agreement with measurements in this region (Harwood et al., 2008). SST and $\delta^{18}O_w$ time
221 series for all cases are given in **S4** and natural cases are plotted in **Fig. 3**.

For all virtual datasets (cases 1-33), records of SST and $\delta^{18}O_w$ were converted to the sampling domain (along the length of the record) by defining a virtual growth rate in the sampling direction. Adding this growth rate as a variable allowed us to test the sensitivity of approaches to changes in the extension rate of the archive, including hiatuses (growth rate = 0). This is important, because fluctuations in linear extension rate and periods in which no mineralization occurs (hiatuses or growth cessations) are common in all climate archives (e.g. Treble et al., 2003; Ivany, 2012). After conversion to the sampling domain, virtual aliquots were subsampled at equal distance from the SST and $\delta^{18}O_w$ series of all cases using six sampling intervals: 0.1 mm, 0.2 mm, 0.45 mm, 0.75 mm, 1.55 mm and 3.25 mm. The four largest sampling intervals were chosen such that the standard growth rate (10 mm/yr) was not an integer multiple of the sampling interval (e.g. 0.45 mm instead of 0.5 mm, and 3.25 mm instead of 3 mm). This decision prevents sampling the same parts of the seasonal cycle (e.g. same months) every year, which biases both the mean value and the precision of monthly SST and $\delta^{18}O_w$ reconstructions. This bias towards certain parts of the seasonal cycle is much stronger at low sample sizes (large sampling intervals) and is illustrated in the **Supplementary Information**.

can you point to a specific figure or supp. discussion section?

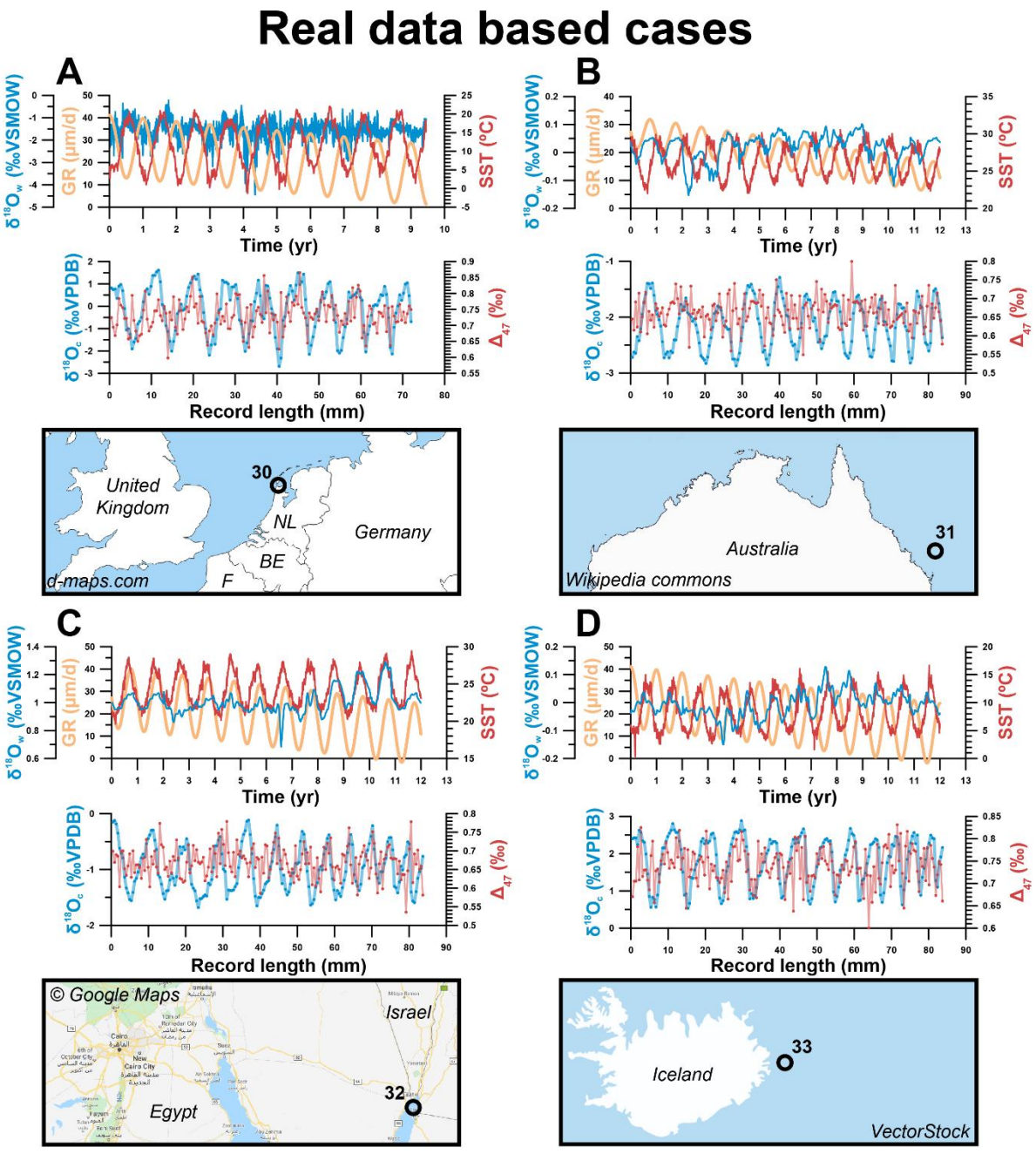

236

237 ***Figure 3**: Overview of the four cases of virtual data based on natural SST and SSS measurements explored*
238 *in this study. (**A**) Case 30: Tidal flats on the Wadden Sea, Texel, the Netherlands. (**B**) Case 31 Great Barrier*
239 *Reef, Australia). (**C**) Case 32: Gulf of Aqaba between Egypt and Saudi Arabia. (**D**) Case 33: Atlantic Ocean*
240 *east of Iceland. For all cases, graphs on top show environmental data, with SST plotted in red, $\delta^{18}O_w$ in*
241 *blue and growth rate (abbreviated as "GR") in orange (as in **Fig. 2**). The graph below shows virtual $\delta^{18}O_c$*
242 *(blue) and Δ_{47} (red) records created from these data series using a sampling interval of 0.45 mm and*
243 *including analytical noise (see **3.3**). Note that the scale of vertical axes varies between plots.*

244

245 *2.3.3 Virtual cases* (virtual environmental data; virtual proxy data)

246 Virtual SST and $\delta^{18}O_w$ time series were artificially constructed to test the effect of various SST and $\delta^{18}O_w$
247 scenarios on the effectivity of the reconstruction methods. The default test case (case 1) contained an ideal,
248 12-year sinusoidal SST curve with a period of 1 year (seasonality), a mean value of 20°C and a seasonal
249 amplitude of 10°C, a constant $\delta^{18}O_w$ value of 0‰ and a constant growth rate of 10 mm/yr. Other cases
250 contain various deviations from this ideal case (see also **Fig. 2**, **Table 1** and **S1**):

251 • Linear and/or seasonal changes in growth rate, including growth stops (cases 2-6, 14-18)
252 • Seasonal and/or multi-annual changes in $\delta^{18}O_w$ (cases 7-11, 13-18)
253 • Multi-annual trends in SST superimposed on the seasonality (cases 12, 15 and 17)
254 • Variations in the seasonal SST amplitude (cases 19-21)
255 • Change in the total length of the time series (cases 22-24).
256 • Variation in uncertainty on the age of each virtual datapoint (cases 25-29)

257 Comparison of the virtual time series (case 1-29; **Fig. 2**) with the natural variability (case 30-33; **Fig. 3**)
258 shows that the virtual cases are not realistic approximations of natural variability in SST and $\delta^{18}O_w$. Natural
259 SST and $\delta^{18}O_w$ variability are not limited to the seasonal or multi-annual scale but contain a fair amount of
260 higher order (daily to weekly scale) variability. To simulate this natural variability, we extracted the seasonal
261 component of SST and $\delta^{18}O_w$ variability from our highest resolution record of measured natural SST and
262 SSS data (case 30: data from Texel, the Netherlands, see **2.3.2** and **Fig. 3**). The standard deviation of
263 residual variability of this data after subtraction of the seasonal cycle was used to add random high-
264 frequency noise to the SST and $\delta^{18}O_w$ variability in virtual cases. Note that while sub-annual environmental
265 variability can be approximated by Gaussian noise (Wilkinson and Ivany, 2002), this representation is an
266 oversimplification of reality. In the case of our Texel data, the SST and SSS residuals are not normally
267 distributed (Kolmogorov-Smirnov test: $D = 0.010$; $p = 7.2*10^{-14}$ and $D = 0.039$; $p < 2.2*10^{-16}$ for SST and
268 SSS residuals respectively; see **S2-4**). SST and $\delta^{18}O_w$ data from cases 1-29 was converted to the sampling
269 domain and subsampled at a range of sampling resolutions following the same procedure applied to cases
270 30-33 (see **2.3.2**).

271

2.4 Conversion to $\delta^{18}O_c$ and Δ_{47} data

After subsampling, SST and $\delta^{18}O_w$ series (cases 1-33) were converted to $\delta^{18}O_c$ and Δ_{47} using a carbonate model based on empirical relationships between Δ_{47} and $\delta^{18}O_c$ with and SST and $\delta^{18}O_w$ (equation 3 and 4; Kim and O'Neil, 1997; Kele et al., 2015; Bernasconi et al., 2018) and the conversion of $\delta^{18}O$ values from VSMOW to VPDB scale (equation 5; Brand et al., 2014).

$$\Delta_{47} = \frac{0.0449*10^6}{(SST+273.15)^2} + 0.167 \qquad (3)$$

$$1000 * \ln \frac{\left({}^{18}O/_{16}O\right)_{CaCO_3}}{\left({}^{18}O/_{16}O\right)_{H_2O}} = 18.03 * \left(\frac{10^3}{(SST+273.15)}\right) - 32.42 \qquad (4)$$

$$\delta^{18}O_{VPDB} = 0.97002 * \delta^{18}O_{VSMOW} - 29.98 \qquad (5)$$

For the real oyster data (Ullmann et al., 2010; see **2.3.1**), only the Δ_{47} data needed to be created because $\delta^{18}O_c$ was directly measured. As a result, each case study yielded records of Δ_{47} and $\delta^{18}O_c$ in the sampling domain and corresponding "true" SST and $\delta^{18}O_w$ records in the time domain, allowing assessment of the reliability of the reconstruction approaches in different scenarios. (**Figure 4**). The result of applying these steps is illustrated on case 31 (Great Barrier reef data, **Fig. 5**). All calculations for creating Δ_{47} and $\delta^{18}O_c$ series in sampling domain were carried out using the open-source computational software R (R core team, 2013), and scripts for these calculations are given in **S7** and compiled in the documented R package "seasonalclumped" (de Winter, 2021a). All Δ_{47} and $\delta^{18}O_c$ datasets are provided in **S6**.

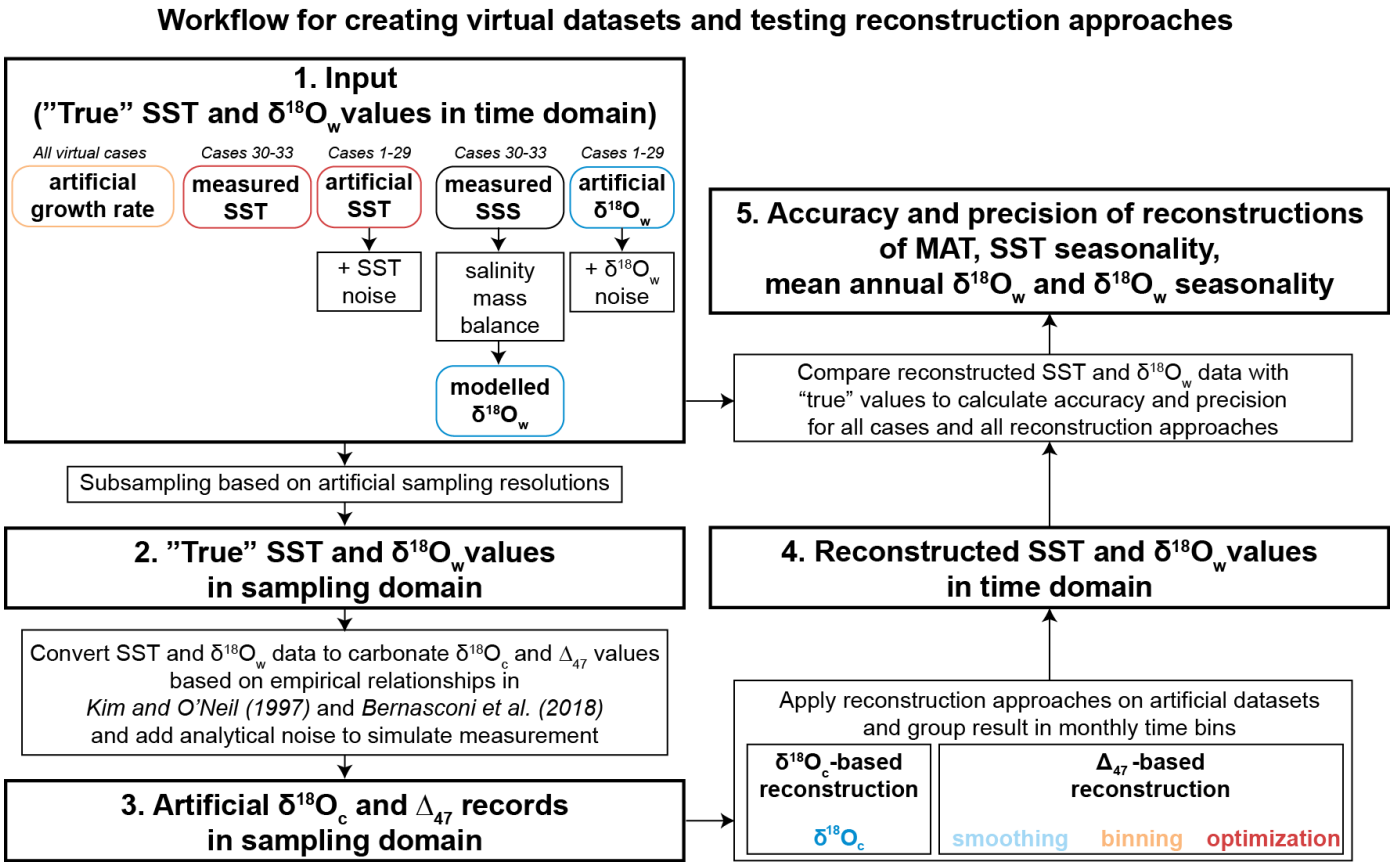

***Figure 4**: Flow diagram showing the steps taken to create virtual data (Δ_{47} and $\delta^{18}O_c$; cases 1-33) and compare results of SST and $\delta^{18}O_w$ reconstructions with the actual SST and $\delta^{18}O_w$ data the record was based on (counterclockwise direction). Steps 1-3 outline the procedure for creating virtual Δ_{47} and $\delta^{18}O_c$ datasets (see sections **2.3** and **2.4**), step 4 shows the application of the different reconstruction methods on this virtual data (see **Fig. 2** for details) and step 5 illustrates how the reconstructions are compared with the original ("true") SST and $\delta^{18}O_w$ data to calculate accuracy and precision of the reconstruction approaches. Note that step 1 is different for cases 1-29 (based on fully artificial SST and $\delta^{18}O_w$ records; **2.3.3**) than for cases 30-33 (SST and $\delta^{18}O_w$ records based on real SST and SSS data; see **2.3.2**).*

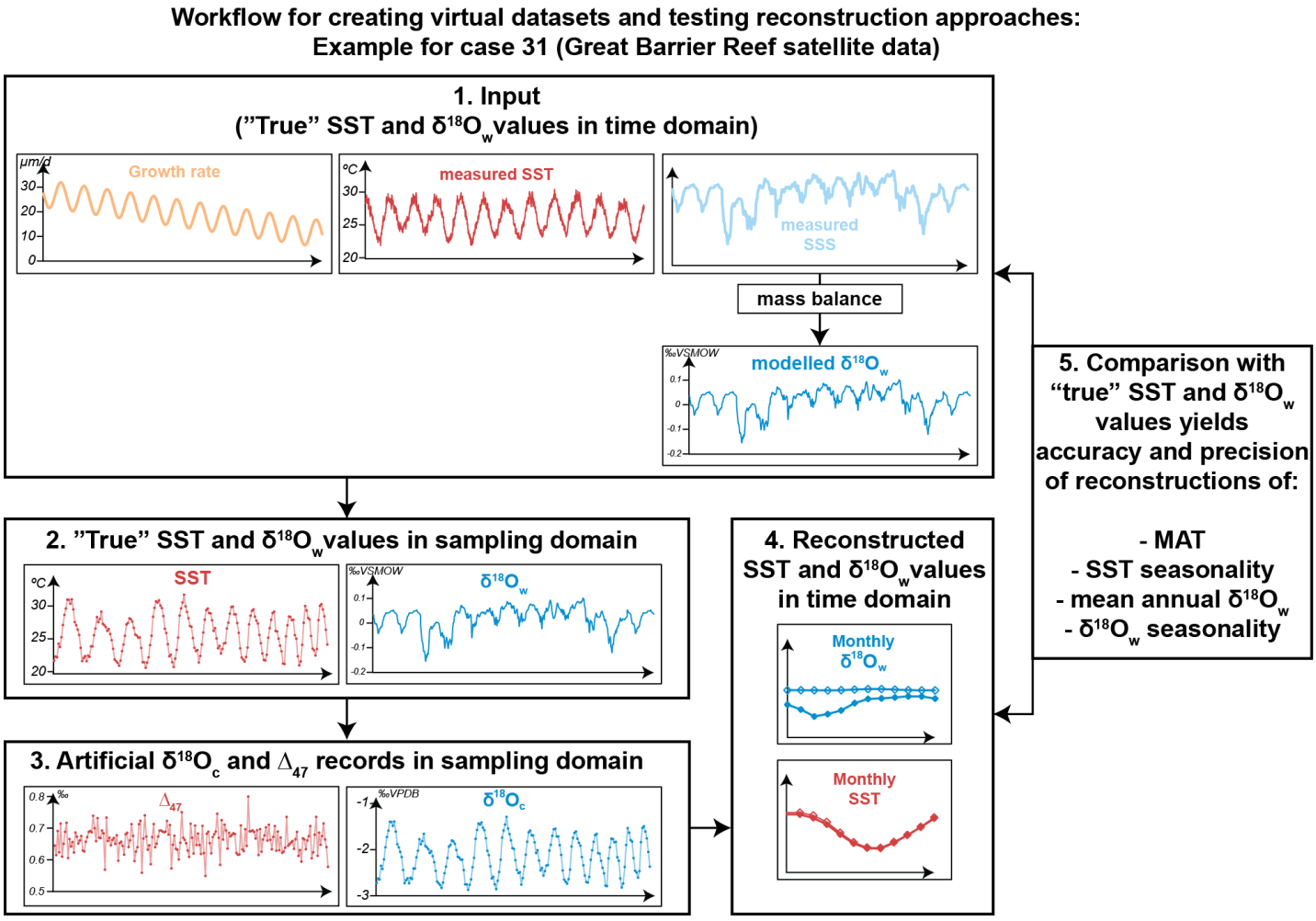

***Figure 5**: An example of the steps highlighted in **Fig. 4** using case 31 (Great Barrier Reef data) to illustrate the data processing steps. Virtual data plots include normally distributed measurement uncertainty on Δ_{47} and $\delta^{18}O_c$*

3. Results

3.1 Real example

Measured ($\delta^{18}O_c$) and simulated (Δ_{47}) data from the Pacific oyster from the Danish List Basin yielded estimates of SST and $\delta^{18}O_w$ seasonality using all reconstruction approaches (**Fig. 6**). While a model of shell $\delta^{18}O_c$ based on SST and SSS data closely approximates the measured $\delta^{18}O_c$ record (**Fig. 6C**), basing SST reconstructions solely on $\delta^{18}O_c$ data without any *a priori* knowledge of $\delta^{18}O_w$ variability (assuming constant $\delta^{18}O_w$ equal to the global marine value) leads to high inaccuracy in SST seasonality and mean annual SST (**Fig. 6D**). The in-phase relationship between SST and SSS (**Fig. 6B**) dampens the seasonal $\delta^{18}O_c$ cycle, causing underestimation of temperature seasonality, while a negative mean annual $\delta^{18}O_w$ value in the List Basin biases SST reconstructions towards higher temperatures. In terms of SST reconstructions, the **smoothing**, **binning** and **optimization** approaches based on Δ_{47} and $\delta^{18}O_c$ data yield more accurate reconstructions, albeit with a reduced seasonality and a bias towards the summer season. The latter is a result of severely reduced growth rates in the winter season, which was therefore undersampled (see **Fig. 6A** and **6C**). Approaches including Δ_{47} data also yield far more accurate $\delta^{18}O_w$ estimates than the **$\delta^{18}O$** approach. However, the accuracy of $\delta^{18}O_w$ seasonality and mean annual $\delta^{18}O_w$ estimates is low in these approaches too, largely because of the limited sampling resolution, especially in winter. The **optimization** approach suffers from the strong in-phase relationship between SST and SSS, which obscures the difference between the $\delta^{18}O_w$ effect and the temperature effect on shell carbonate. Yet, disentangling SST from $\delta^{18}O_w$ seasonality is central to the success of the approach (see **3.4**). **Fig. 6D** does not show the reproducibility error on SST and $\delta^{18}O_w$ estimates, which is much larger for the **smoothing** approach than for the **binning** an **optimization** approaches due to the limited data in the winter seasons (see **S5**). These results show that several properties of carbonate archives, such as growth rate variability, phase relationships between SST and $\delta^{18}O_w$ seasonality and sampling resolution, can impact the reliability of paleoseasonality reconstructions. The virtual and real data cases in this study were tailored to test the effects of these archive properties more thoroughly.

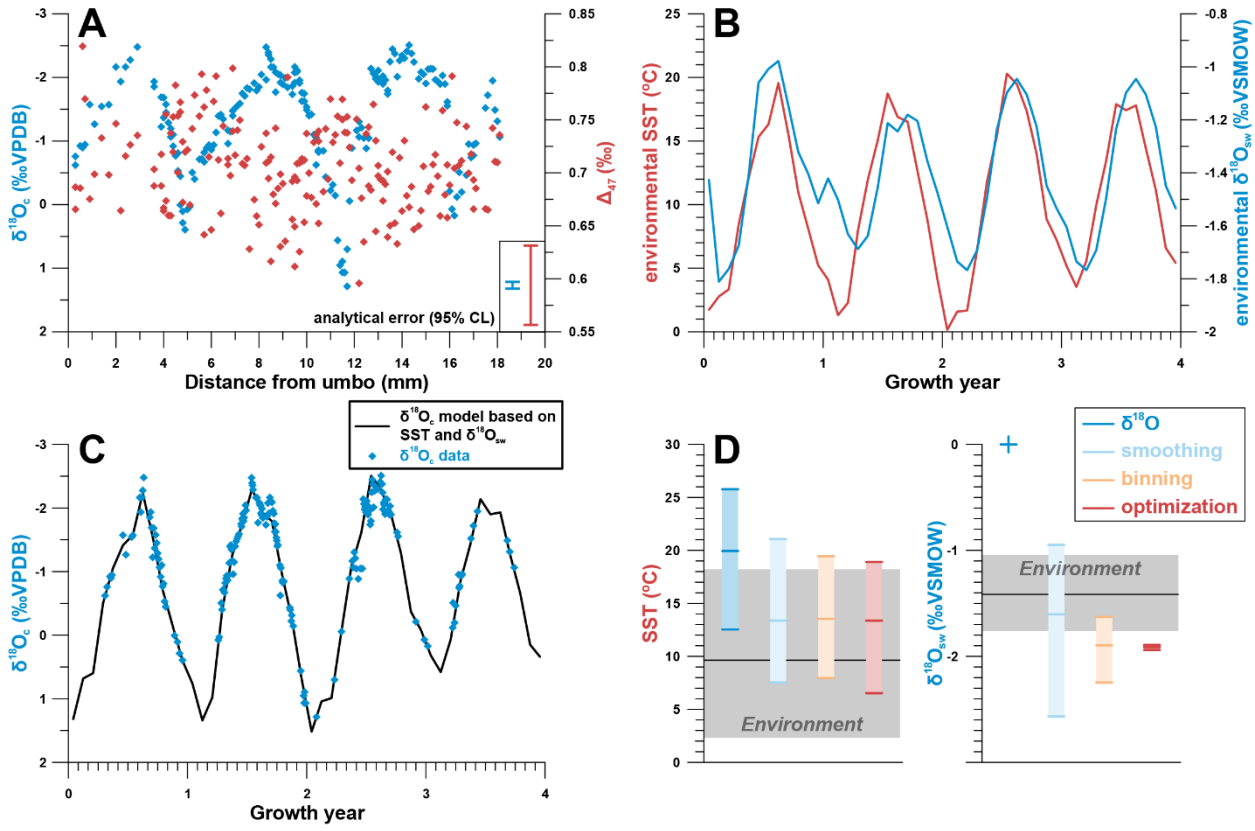

***Figure 6**: (**A**) Plot of $\delta^{18}O_c$ and (virtual) Δ_{47} data from a modern Pacific oyster (*Crassostrea gigas*; see Ullmann et al., 2010). (**B**) shows SST and $\delta^{18}O_w$ data from the List Basin (Denmark) in which the oyster grew. (**C**) shows the fit between $\delta^{18}O_c$ data and modelled $\delta^{18}O_c$ calculated from SST and $\delta^{18}O_w$ on which the shell age model was based. (**D**) Shows a summary of the results of different approaches for reconstructing SST and $\delta^{18}O_w$ from the $\delta^{18}O_c$ and Δ_{47} data. The vertical colored bars show the reconstructed seasonal variability using all methods with ticks indicating warmest month, coldest month, and annual mean. The grey horizontal bars show the actual seasonal variability in the environment. Precision errors on monthly reconstructions are not shown but are given in **S4**.*

see comment in Section 3.3 re: "precision error" terminology

3.2 Case-specific results

A case-by-case breakdown of the precision (**Fig. 7**) and accuracy (**Fig. 8**) of reconstructions using the four approaches shows that reliability of reconstructions varies significantly between approaches and is highly case-specific. In general, precision is highest in **$\delta^{18}O$** reconstructions, followed by **optimization** and **binning** with **smoothing** generally yielding the worst precision. Average precision standard deviations of the underperforming methods (**binning** and **smoothing**) are up to 2-3 times larger than those of **$\delta^{18}O$** (e.g. respectively 3.9°C and 3.5°C vs. 1.3°C for **$\delta^{18}O$** MAT reconstructions; see also **Supplementary Information**). It is worth noting that precision on **$\delta^{18}O$**-based estimates is mainly driven by measurement

Is this redundant in this context?

346 precision (which is better for $\delta^{18}O_c$ than for Δ_{47} measurements, see section **4.1.1**). Δ_{47}-based reconstructions
347 lose precision due to the higher measurement error on Δ_{47} measurements and the method used for
348 combining measurements for seasonality reconstructions. On a case-by-case basis, the hierarchy of
349 approaches can vary, especially if strong variability in growth rate is introduced, such as in case 14, where
350 the size of hiatuses in the record increases progressively, or in case 18, in which half of the year is missing
351 due to growth hiatuses (see **Table 1**, **S1** and **S4**). Of the Δ_{47}-based methods (**smoothing**, **binning** and
352 **optimization**), **optimization** is rarely outcompeted in terms of precision in both SST and $\delta^{18}O_w$
353 reconstructions.

354 The comparison based on precision alone is misleading, as the most precise approach (**$\delta^{18}O$**) runs the risk
355 of being highly inaccurate (offsets exceeding 4°C on some MAT reconstructions; see **Fig. 7C**), especially
356 in cases based on natural SST and SSS (case 30-33). The **smoothing** approach also often yields highly
357 inaccurate results, especially in cases with substantial variability in $\delta^{18}O_w$ (e.g. case 9-11). Accuracy of
358 **optimization** and **binning** outcompete the other methods in most circumstances. **Binning** outperforms
359 **optimization** in reconstructions of $\delta^{18}O_w$ seasonality, making it overall the most accurate approach.
360 Interestingly, **optimization** is less accurate specifically in cases with sharp changes in growth rate in
361 summer (e.g. cases 11, 14, 16 and 17), while **binning** performs better in these cases. Reconstructions of
362 mean annual SST and $\delta^{18}O_w$ in case 18 are especially inaccurate regardless of which method is applied.
363 This extreme case with growth only during one half of the year combined with seasonal fluctuations in both
364 SST and $\delta^{18}O_w$ presents a worst-case scenario for seasonality reconstructions leading to strong biases in
365 mean annual temperature reconstructions. In situations like case 18, the **optimization** approach is most
366 accurate in MAT and SST seasonality reconstructions, but $\delta^{18}O_w$ is more accurately reconstructed using
367 the **binning** approach. Finally, it is worth noting that in natural situations (**Fig. 3**), variability in SST almost
368 invariably has a larger influence on $\delta^{18}O_c$ and Δ_{47} records than $\delta^{18}O_w$, such that fluctuations in $\delta^{18}O_c$ records
369 closely follow the SST seasonality even in cases with relatively large $\delta^{18}O_w$ variability (e.g. case 30).
370 Chronologies based on these $\delta^{18}O_c$ fluctuations are therefore generally accurate.

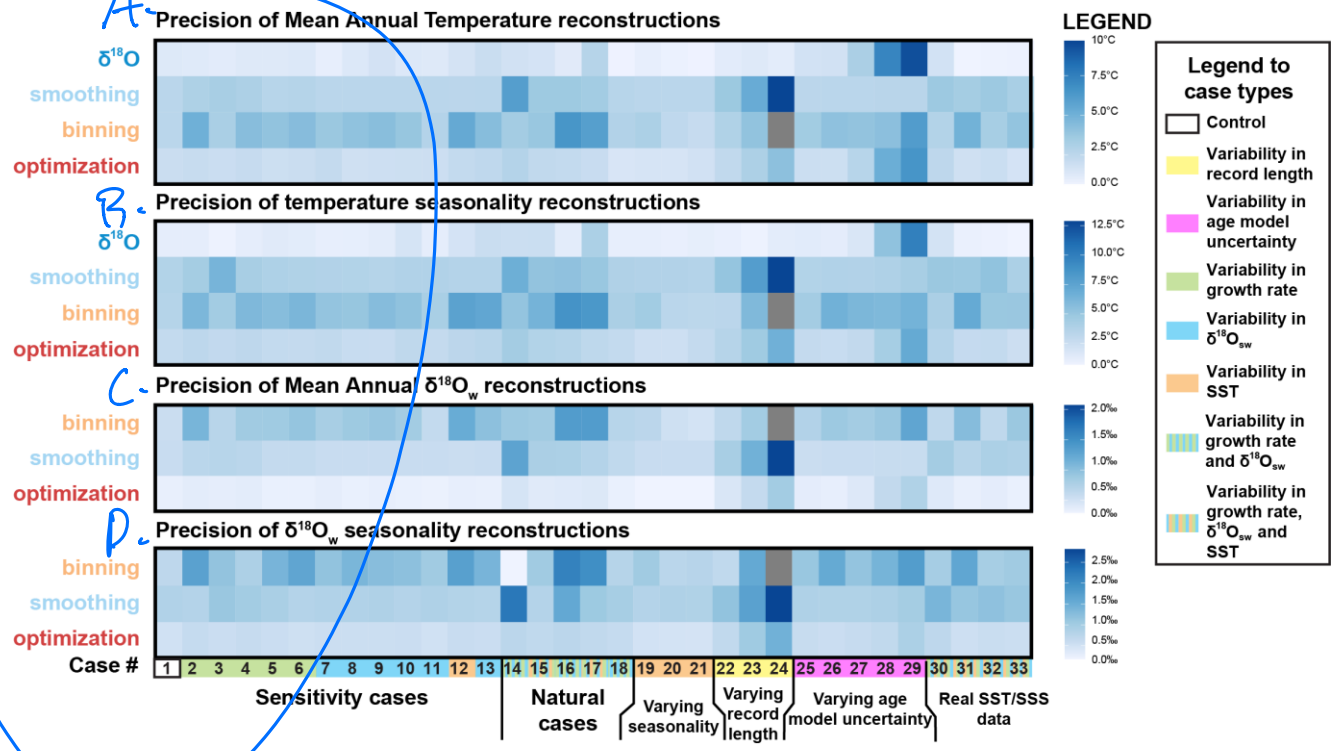

***Figure 7**: Overview of precision (propagated standard deviation of variability within reconstructions, see **2.2**) of reconstructions of mean annual temperature (**A**), seasonal temperature range (**B**), mean annual $\delta^{18}O_w$ (**C**) and seasonal range in $\delta^{18}O_w$ (**D**), with higher values (darker colors) indicating lower precision (more variability between reconstructions) based on average sampling resolution (sampling interval of 0.45 mm). The different cases on the horizontal axis are color coded by their difference from the control case (case 1; see legend on the right-hand side). Grey boxes indicate cases for which reconstructions were not successful. All data on precision (standard deviation values) is provided in **S4**.*

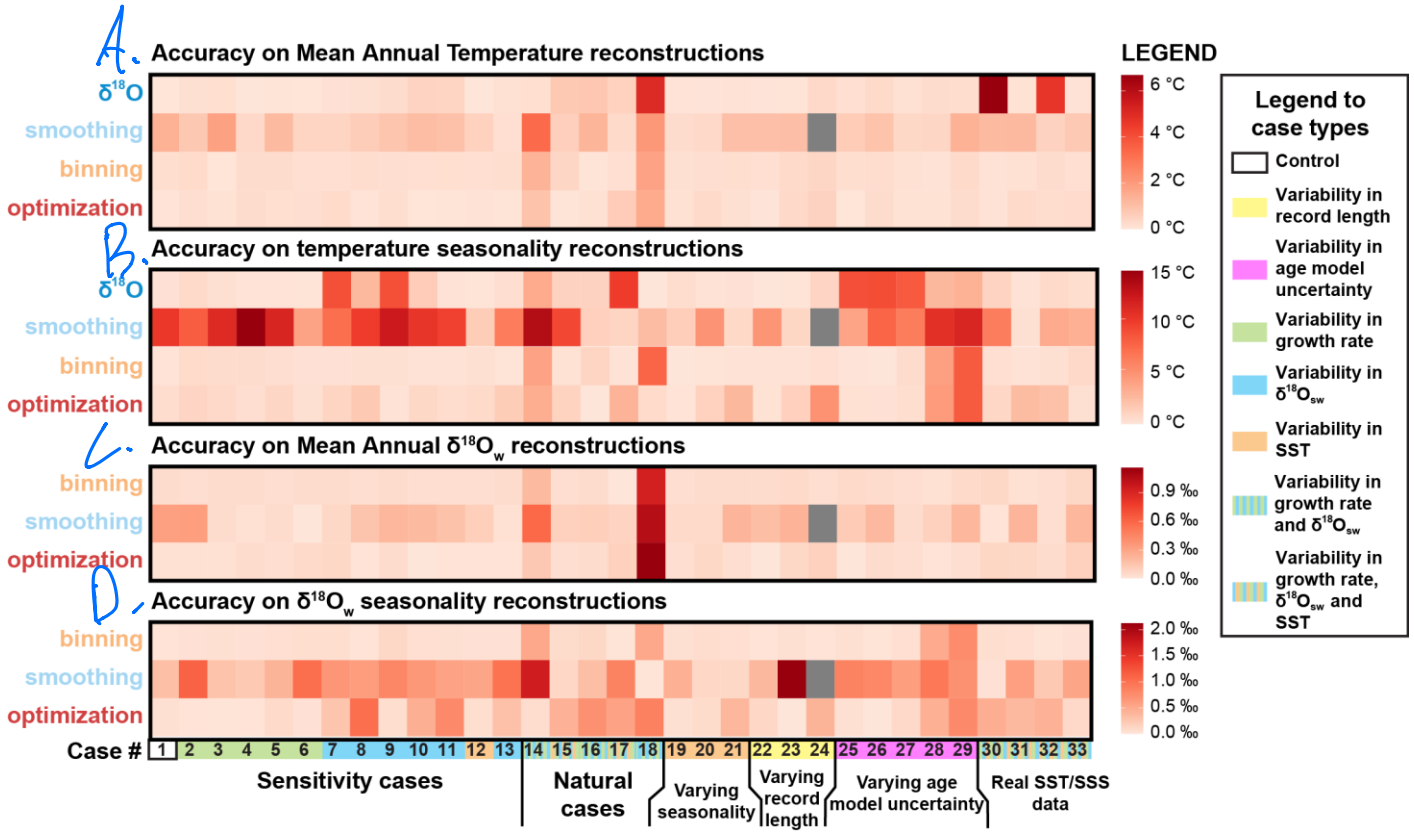

***Figure 8**: Overview of accuracy (absolute offset from "true" values) of reconstructions of mean annual temperature (**A**), seasonal temperature range (**B**), mean annual $\delta^{18}O_w$ (**C**) and seasonal range in $\delta^{18}O_w$ (**D**), with higher values (darker colors) indicating lower accuracy (higher offsets) based on average sampling resolution (sampling interval of 0.45 mm). The different cases on the horizontal axis are color coded by their difference from the control case (case 1; see legend on the right-hand side). Grey boxes indicate cases for which reconstructions were not successful. All data on accuracy (difference between reconstructed and "true" values) is provided in **S4**.*

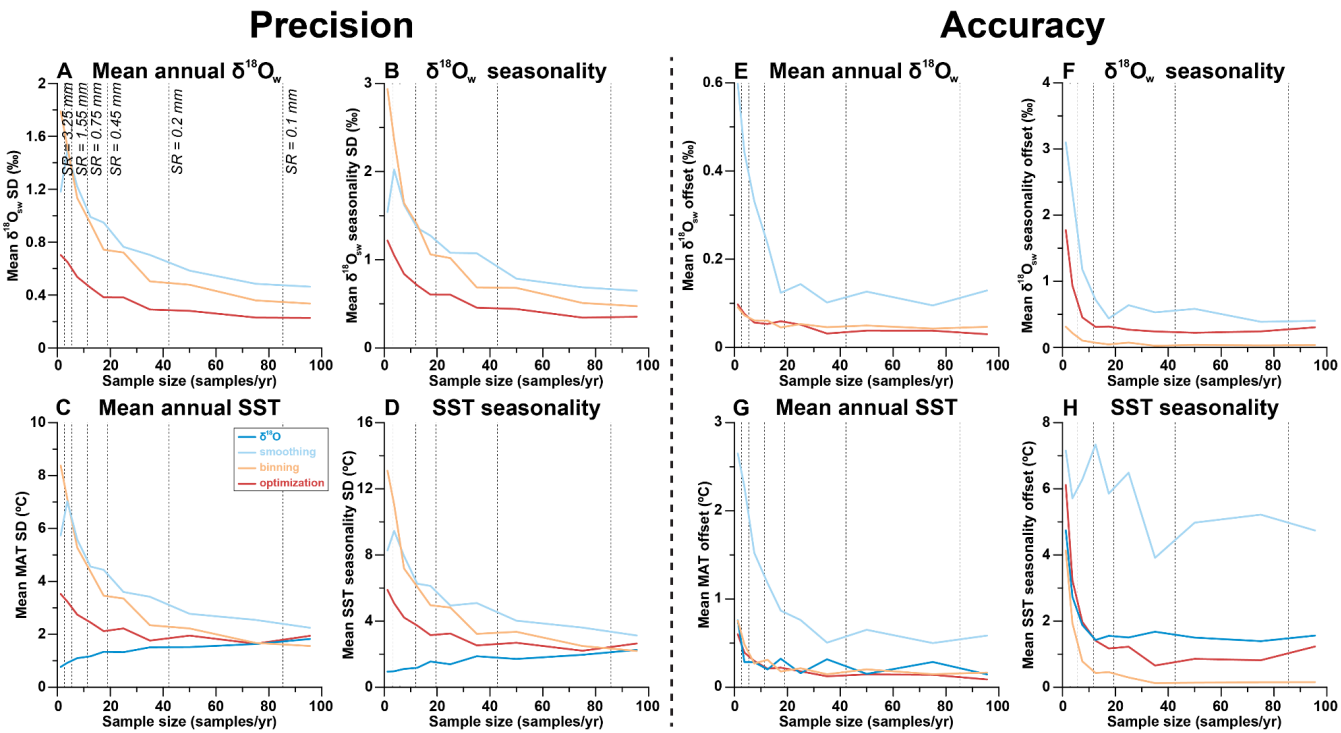

***Figure 9**: Effect of sampling resolution (in samples per year, see **S5**) on the precision (one standard deviation) of results of reconstructions of mean annual $\delta^{18}O_w$ (**A**), seasonal range in $\delta^{18}O_w$ (**B**), mean annual SST (**C**) and seasonal range in SST (**D**). Effect on the accuracy (absolute offset from actual value) of results of reconstructions of mean annual $\delta^{18}O_w$ (**E**) and seasonal range in $\delta^{18}O_w$ (**F**), mean annual SST (**G**) and seasonal range in SST (**H**). Color coding follows the scheme in **Fig. 1** and **Fig. 4**.*

3.3 Effect of sampling resolution

As expected, increasing the temporal sampling resolution (i.e. number of samples per year) almost invariably increases the precision and accuracy (**Fig. 9**) of reconstructions using all methods. An exception to this rule is the precision of $\delta^{18}O$ reconstructions, which decreases with increasing sampling resolution. Precision errors of all Δ_{47}-based approaches eventually converge with the initially much lower precision error of $\delta^{18}O$ reconstructions when sampling resolution increases. However, the sampling resolution required for Δ_{47}-based reconstructions to rival or outcompete the $\delta^{18}O$ reconstructions differs, with **optimization** requiring lower sampling resolutions than the other methods (e.g. 20-40 samples/year compared to 40-80 samples/year for **smoothing** and **binning**; **Fig. 9A-D**). Accuracy also improves with sampling resolution (**Fig. 9E-H**). When grouping all cases together, it becomes clear that $\delta^{18}O$ reconstructions can only approach the accuracy of Δ_{47}-based approaches for reconstructions of MAT. Seasonality in both SST and $\delta^{18}O_w$ is most accurately reconstructed using **binning**, and the **smoothing** approach once again performs worst.

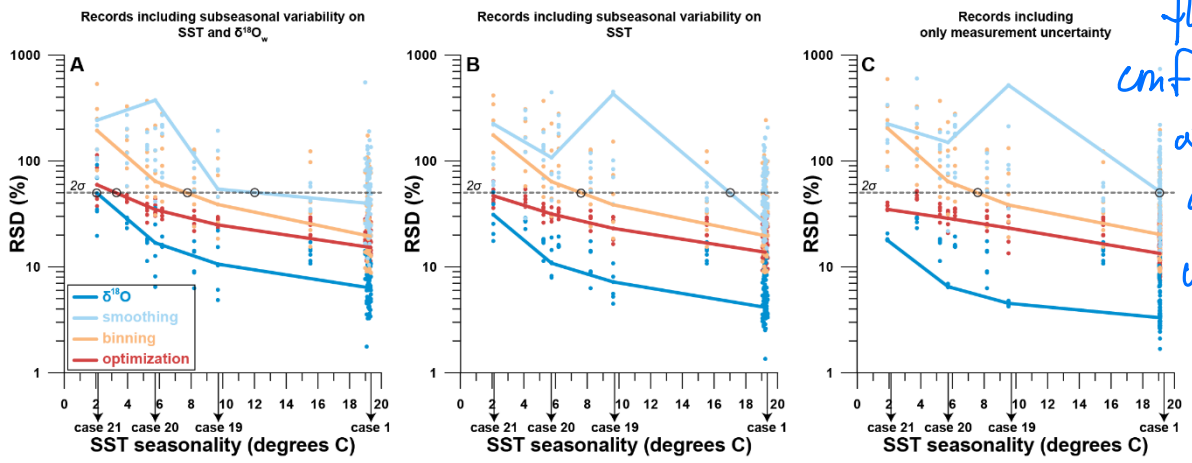

***Figure 10**: Effect of SST seasonality range (difference between warmest and coldest month) in the record on the relative precision of SST seasonality reconstructions ("RSD", defined as one standard deviation divided by the mean value). Panel **A** shows precision results if random variability ("weather patterns") in both SST and $\delta^{18}O_w$ as well as measurement uncertainty is added to the records (see **2.3.3** and **S1**). Panel **B** shows precision of records with random variability in SST and measurement uncertainty only. Panel **C** shows precision if only measurement uncertainty is considered. Color coding follows the scheme in **Fig. 1** and **Fig. 4**. Shaded dots represent results at various sampling resolutions, while bold lines are averages for all reconstruction approaches. Black circles highlight the places where curves cross the threshold of two standard deviations, which indicates the minimum SST seasonality that can be resolved within 2 standard deviations (~95% confidence level) using the reconstruction approach.*

3.4 Resolving SST seasonality

Comparison of cases 19, 20 and 21 (SST seasonality of 9.7°C, 5.7°C and 2.1°C respectively) with control case 1 (SST seasonality of 19.3°C) shows how changes in the seasonal SST range affect the precision of measurements (**Fig. 10**; see also **Table 1** and **S1**). The data reconfirms that **$\delta^{18}O$** reconstructions are most precise; a deceptive statistic given the risk of highly inaccurate results this approach yields (see **Fig. 8**). Taking into consideration only analytical uncertainty, all approaches except for **smoothing** can confidently resolve at least the highest SST seasonality within a significance level of two standard deviations (~95%) using a moderate sampling resolution (mean of all resolutions shown in **Fig. 10**). Increasing sampling resolution improves the precision of Δ_{47}-based reconstructions (see **Fig. 9D**), so high sampling resolutions (0.1 or 0.2 mm) allow smaller seasonal differences to be resolved. When random sub-annual variability is added to the SST and $\delta^{18}O_w$ records (see **2.3.3**), the minimum seasonal SST extent that can be resolved decreases for all approaches (**Fig. 10B** and **10C**). Nevertheless, **$\delta^{18}O$** and **optimization** reconstructions remain able to resolve a relatively small SST seasonality of 2-4°C.

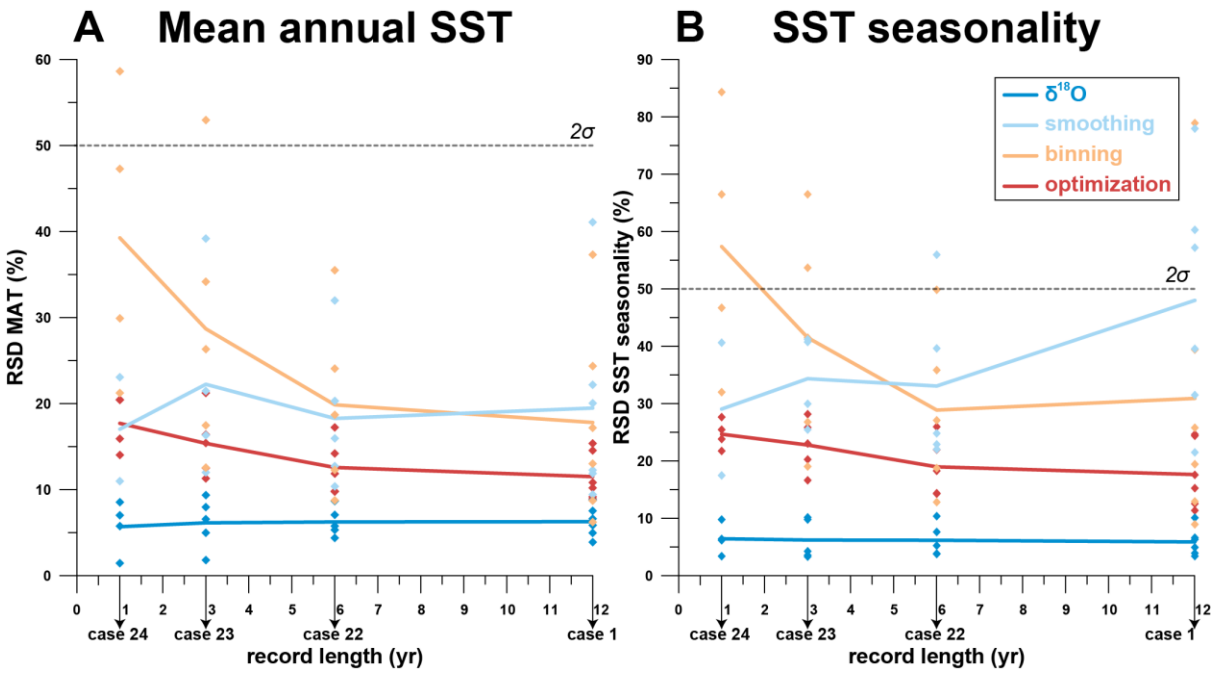

***Figure 11**: Effect of record length (in years) on the relative precision (one standard deviation as fraction of the mean value) of results of reconstructions of mean annual SST (**A**) and SST seasonality (**B**). Shaded dots represent results for the six different sampling resolutions. Solid lines connect averages for cases 1, 22, 23 and 24 for each reconstruction approach.*

3.5 Effect of record length

The effect of variation in the length of the record was investigated by comparing cases 22, 23 and 24 (record lengths of 6 years, 3 years and 1 year, respectively) with the control case (record length of 12 years; see **Fig. 11** and **Table 1**). Precision of MAT and SST seasonality reconstructions slightly increase in larger datasets (longer records) for **optimization** and **binning**, but not for **smoothing** and **$\delta^{18}O$** reconstructions. Differences between reconstruction approaches remain relatively constant regardless of the length of the record, with general precision hierarchy remaining intact (**$\delta^{18}O$** > **optimization** > **binning** > **smoothing**). However, in very short records (1-2 years) **smoothing** gains an advantage over other Δ_{47}-based methods due to its lack of sensitivity to changes in the record length and **binning** reconstructions are not precise enough to resolve MAT and SST seasonality within two standard deviations (~95% confidence level). Variation in precision is largely driven by very high precision errors of reconstructions in records with low sampling resolutions (sampling intervals of 1.55 mm or 3.25 mm; see also **Fig. 9A-D**). As a result, most of the reduction in precision in shorter records can be mitigated by denser sampling.

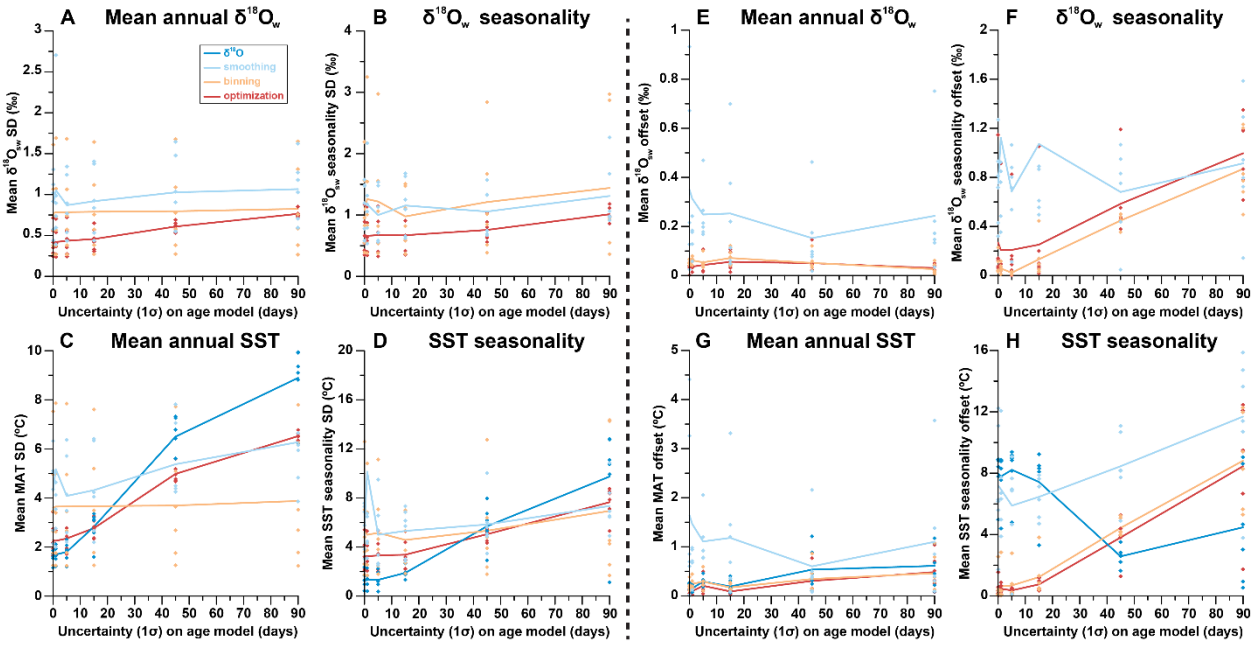

***Figure 12**: Effect of uncertainty in age model on the reproducibility (standard deviation on estimate) of results of reconstructions of mean annual $\delta^{18}O_w$ (**A**) and seasonal range in $\delta^{18}O_w$ (**B**), mean annual SST (**C**) and seasonal range in SST (**D**). Effect of uncertainty in age model on the accuracy (offset from true value) of results of reconstructions of mean annual $\delta^{18}O_w$ (**E**) and seasonal range in $\delta^{18}O_w$ (**F**), mean annual SST (**G**) and seasonal range in SST (**H**). Color coding follows the scheme in **Fig. 1** and **Fig. 4**.*

3.6 Effect of age model uncertainty

Uncertainty on the age model has a significant effect on both the precision and the accuracy (**Fig. 12**) of reconstructions using all approaches. The **$\delta^{18}O$** reconstructions are most strongly affected by uncertainties in the age model and suffer from a large decrease in precision with increasing age model uncertainty (**Fig. 12C-D**). The high reproducibility of the **$\delta^{18}O$** approach in comparison with the Δ_{47} approaches quickly disappears when age model uncertainty increases beyond 20-30 days. Accuracy of $\delta^{18}O_c$-based SST seasonality reconstructions initially improves with age model uncertainty (**Fig. 12H**). However, this observation is likely caused by the fact that age model uncertainty was compared based on conditions in case 9, which features a phase offset between SST and $\delta^{18}O_w$ seasonality causing the **$\delta^{18}O$** method to be highly inaccurate even without age model uncertainty. The precision of **smoothing** and **optimization** approaches also decreases with increasing age model uncertainty (**Fig 12A-D**), and the **optimization** approach loses its precision advantage over the **binning** and **smoothing** approaches when age model uncertainty increases beyond 30 days. The monthly **binning** approach is most resilient against increasing age model uncertainty. Seasonality reconstructions through both the **binning** and **optimization** approach quickly lose accuracy when age model uncertainty increases but the accuracy of the **smoothing** approach remains the worst of all approaches in regardless of age model uncertainty (**Fig. 12E-H**).

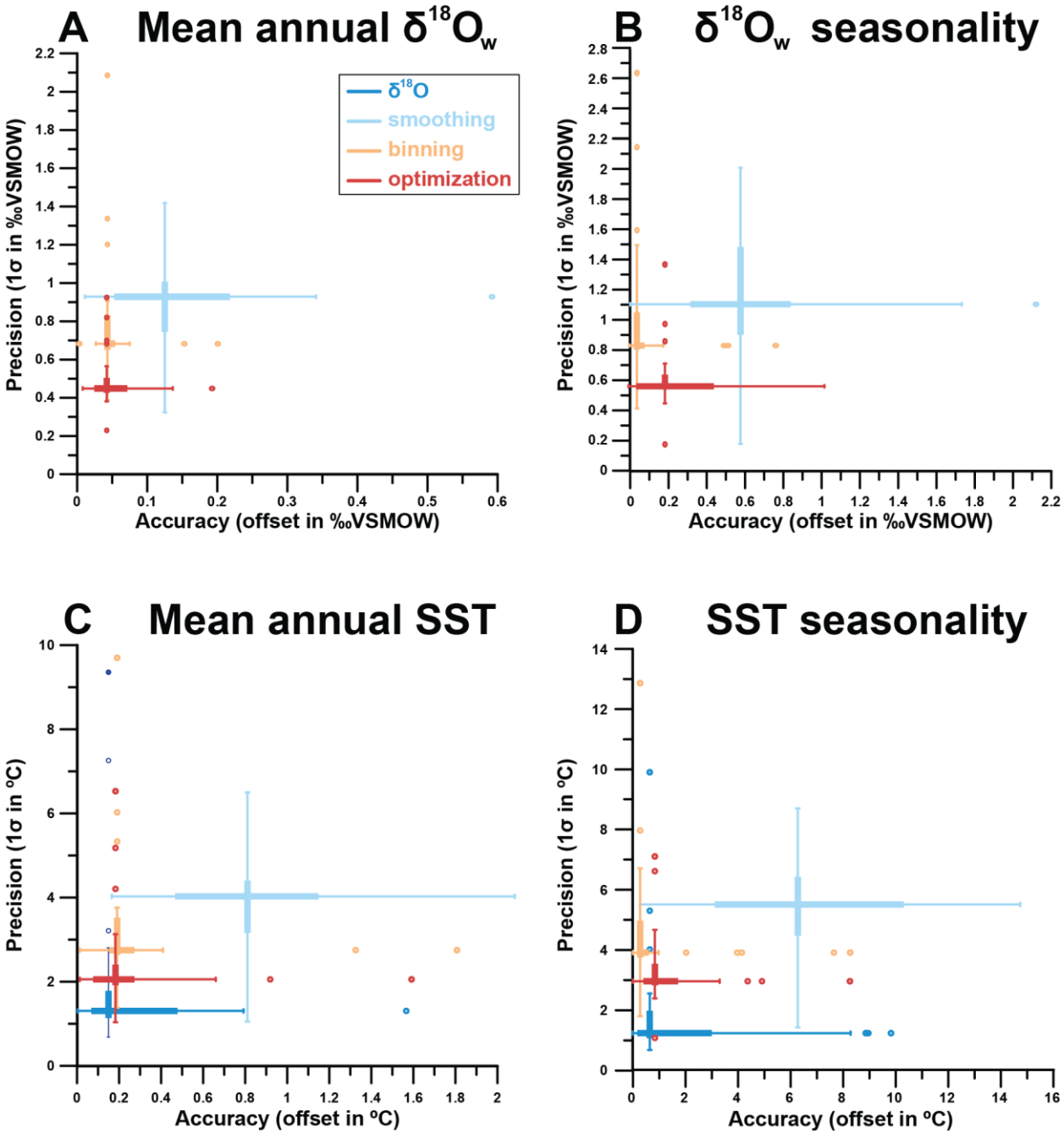

***Figure 13**: Overview of averages and ranges of accuracy (absolute offset from real value) and precision (one standard deviation from the mean) on mean annual $\delta^{18}O_w$ (**A**) and seasonal range in $\delta^{18}O_w$ (**B**), mean annual SST (**C**) and seasonal range in SST (**D**) within all cases using the four different reconstruction approaches. Color coding follows the scheme in **Fig. 1** and **Fig. 4**. Box-whisker plots for precision and accuracy cross at their median values and outliers (colored symbols) are identified based on 2x the interquartile difference.*

4. Discussion

4.1 Performance of reconstruction approaches

4.1.1 $\delta^{18}O_c$ vs Δ_{47}-based reconstructions

Figure 13 summarizes the general reliability of the four approaches. **$\delta^{18}O$** reconstructions are generally less accurate than Δ_{47}-based reconstructions (especially **binning** and **optimization**; see also **S9**). This is a consequence of the assumption that $\delta^{18}O_w$ remains constant year-round, and that one knows its true value. Both these assumptions are problematic in absence of independent evidence of the value of $\delta^{18}O_w$, especially in deep time settings (see e.g. Veizer and Prokoph, 2015; Henkes et al., 2018). The risk of this assumption is made clear when comparing cases in which $\delta^{18}O_w$ is indeed constant year-round at the assumed value (0‰; e.g. cases 1-6 and 19-24) with cases in which shifts in $\delta^{18}O_w$ occur, especially when these shifts are out of phase with respect to the SST seasonality (e.g. cases 9-11, 18 and 25-33; **Fig. 8C-D**). Cases mimicking or based on natural SST and SSS variability (cases 14-18 and 30-33) as well as the modern oyster data (**Fig. 6**) yield stronger inaccuracies in MAT and seasonality reconstructions, showing that even in many modern natural circumstances the assumption of constant $\delta^{18}O_w$ is problematic.

It is important to consider that the value of mean annual $\delta^{18}O_w$ remained very close to the assumed value of 0‰ (within 0.15‰) in all cases except for natural data cases 30 (-1.55‰), 32 (1.01‰; see **S5**) and the real oyster data (-1.42‰; **Fig. 5**). The SST values of these cases reconstructed using $\delta^{18}O_c$ data show large offsets from their actual values (+6.7°C, -4.7°C and +10.3°C for case 30, case 32 and the real oyster data respectively; see **Fig. 6 and 8** and **S5**). These offsets are equivalent to the temperature offset one might expect from inaccurately estimating $\delta^{18}O_w$ (~-4.6 °C/‰; Kim and O'Neil, 1997) and are only rivaled by the offset in MAT reconstructions of case 18 (+5.0°C), which has growth hiatuses obscuring the coldest half of the seasonal cycle. The fact that such differences in $\delta^{18}O_w$ exist even in modern environments should not come as a surprise, given the available data on variability of $\delta^{18}O_w$ (at least -3‰ to +2‰; e.g. LeGrande and Schmidt, 2006) and SSS (30 to 40; ESA, 2020) in modern ocean basins. However, it should warrant caution in using $\delta^{18}O_c$ data for SST reconstructions even in modern settings. Implications for deep time reconstructions are even greater, given the uncertainty on and variability in global average (let alone local) $\delta^{18}O_w$ values (Jaffrés et al., 2007; Veizer and Prokoph, 2015). The complications of using $\delta^{18}O_c$ as a proxy

for marine temperatures in deep time are discussed in detail in O'Brien et al. (2017), and Tagliavento et al. (2019).

The analytical uncertainty of individual $\delta^{18}O_c$ aliquots (typically 1 S.D. of 0.05‰; e.g. de Winter et al., 2018) represents only ~1.1% of the variability in $\delta^{18}O_c$ over the seasonal cycle (~4.3‰ for the default 20°C seasonality in case 1, following Kim and O'Neil, 1997). This is much smaller than the analytical uncertainty of Δ_{47} (typically 1 S.D. of 0.02-0.04‰; e.g. Fernandez et al., 2018; de Winter et al., 2020b), which equates to 25-50% of the seasonal variability in Δ_{47} (~0.08‰ for 20°C seasonality, following Bernasconi et al., 2018; see **S7**). This roughly 20-fold difference in relative precision causes $\delta^{18}O_c$ based SST reconstructions to be much more precise (see **Figs 7**, **9-12**) than those based on Δ_{47}, and forces the necessity for grouping Δ_{47} data in reconstructions. However, as discussed above, the high precision of **$\delta^{18}O$** reconstructions is a misleading statistic if they are highly inaccurate.

Our results show that paleoseasonality reconstructions based on $\delta^{18}O_c$ can only be relied upon if there is strong independent evidence of the value of $\delta^{18}O_w$ and if significant sub-annual variability in $\delta^{18}O_w$ (>0.3‰, equivalent to a 2-3°C SST variability; see **Fig. 9-10**; Kim and O'Neil, 1997) can be excluded with confidence. Examples of such cases include fully marine environments unaffected by influxes of (isotopically light) freshwater or evaporation (increasing $\delta^{18}O_w$; Rohling, 2013). Carbonate records from environments with more stable $\delta^{18}O_w$ conditions include, for example, the *A. islandica* bivalves from considerable depth (30-50m) in the open marine Northern Atlantic (e.g. Schöne et al., 2005, on which case 33 is based). However, even here variability in $\delta^{18}O_{sw}$ due to, for example, shifting influence of different bottom water masses cannot be fully excluded. Previous reconstruction studies show that $\delta^{18}O_w$ in smaller basins are heavily influenced by the processes affecting $\delta^{18}O_w$ on smaller scales, such as local evaporation and freshwater influx from nearby rivers (e.g. Surge et al., 2001; Petersen et al., 2016). Consequently, accurate quantitative reconstructions of seasonal range in shallow marine environments with extreme seasonality may not be feasible using the **$\delta^{18}O$** approach, because these environments are invariably characterized by significant fluctuations in $\delta^{18}O_w$ and growth rate.

While variability in $\delta^{18}O_w$ compromises accurate $\delta^{18}O$-based seasonality reconstructions, the compilation in **Fig. 3** shows that its influence on the $\delta^{18}O$ records is too small to affect the shape of the record to such

a degree that seasonality is fully obscured. While natural situations with $\delta^{18}O_w$ fluctuations large enough to totally counterbalance the effect of temperature seasonality on $\delta^{18}O$ records are imaginable, these cases are likely rare. This means that chronologies based on $\delta^{18}O$ seasonality, which are a useful tool to anchor seasonal variability in absence of independent growth markers (e.g. Judd et al., 2018; de Winter, 2021b), are reliable in most natural cases.

*4.1.2 Seasonality reconstructions using moving averages (**smoothing**)*

Of the three methods for combining Δ_{47} data, the **smoothing** approach clearly performs worst in all four reconstructed parameters (MAT, SST seasonality, mean annual $\delta^{18}O_w$ and $\delta^{18}O_w$ seasonality), both in terms of accuracy and precision (**Fig. 13**). While applying a moving average may be a good strategy for lowering the uncertainty of Δ_{47}-based temperature reconstructions in a long time series (e.g. Rodríguez-Sanz et al., 2017), the method underperforms in cases where baseline and amplitude of a periodic component (e.g. MAT and SST seasonality) are extracted from a record. This is likely due to the smoothing effect of the moving average, which reduces the seasonal cycle and causes highly inaccurate seasonality reconstructions (offsets mounting to >6°C; **Fig. 13**). This bias is especially detrimental in cases where the seasonal cycle is obscured by seasonal growth halts (e.g. case 18), multi-annual trends in growth (e.g. case 4, 14 and 17) and multi-annual trends in SST (e.g. case 15 and 17; see **Fig. 7 and 8**). The poor performance of the **smoothing** approach can be slightly mitigated by increasing sampling resolution (**Fig 9**), but even at high sampling resolutions (every 0.1 or 0.2 mm) the method still fails to reliably resolve seasonal SST ranges below 5°C even in idealized cases (case 19-21; **Fig. 10**). Increasing the number of samples by analyzing longer records does not improve the result, because smoothing of the seasonal cycle by a moving average window introduces the same dampening bias if the temporal sampling resolution (number of samples per year) remains equal (**Fig. 11**).

More critically, employing the **smoothing** method may give the illusion that seasonality is more reduced, and severely bias reconstructions. This bias highlights the importance of using the official meteorological definition of seasonality as the difference between the averages of warmest and coldest month in paleoseasonality work (O'Donnell et al., 2012). This definition is much more robust than the "annual range" often cited based on maxima and minima in $\delta^{18}O_c$ records. This "annual range" strongly depends on

sampling resolution, which is typically <12 samples/yr (Goodwin et al., 2003), equivalent to the third lowest sampling interval (0.75 mm) simulated in this study. Therefore, we strongly recommend future studies to adhere to the monthly definition of seasonality to foster comparison between studies. While inter-annual variability is lost by combining data from multiple years into monthly averages, this approach increases precision, accuracy and comparability of paleoseasonality results. Inter-annual variability can still be discussed from plots of raw data plotted in time or sampling domain.

*4.1.3 Monthly **binning**, sample size **optimization** and age model uncertainty*

Overall, the most reliable paleoseasonality reconstructions can be obtained from either **binning** or **optimization** (**Fig. 13**). In general, **optimization** is slightly more precise, while **binning** yields more accurate estimates of seasonal range in SST and $\delta^{18}O_w$ (**Fig. 13B and D**). The more flexible combination of aliquots in the **optimization** routine yields improved precision (especially on mean annual averages) in cases where parts of the record are undersampled or affected by hiatuses and simultaneous fluctuations in both SST and $\delta^{18}O_w$ (e.g. case 3-6, 14-18, 30-33). The downside of this flexibility is that in case of larger sample sizes, the seasonal variability may be dampened, like in the **smoothing** approach (see **4.1.2**). This apparent dampening effect may be reduced by allowing the sample size of summer and winter samples to vary independently in the **optimization** routine, at the cost of higher computational intensity due to the larger number of sample size combinations (see 2.1 and 4.2.2). The rigid grouping of data in monthly bins in **binning** prevents this dampening and therefore yields slightly more accurate estimates of seasonal ranges in SST and $\delta^{18}O_w$. A caveat of **binning** is that it requires a very reliable age model of the record, at least on a monthly scale. If the age model has a large uncertainty, there is a risk that samples are grouped in the wrong month, which compromises the accuracy of **binning** reconstructions, especially for reconstructions of seasonal range (**Fig 12H**). This problem is exacerbated by potential phase shifts between seasonality in paleoclimate variables (SST and $\delta^{18}O_w$) and calendar dates, which may occur in the presence of a reliable age model.

Previous authors attempted to circumvent the dating problem by analyzing high-resolution $\delta^{18}O_c$ transects and subsequently sampling the seasonal extremes for clumped isotope analyses (Keating-Bitonti et al., 2011; Briard et al., 2020). While this approach does not require sub-annual age models, it has several

591 disadvantages compared with the **binning** and **optimization** approaches: Firstly, it requires separate
592 sampling for $\delta^{18}O_c$ and Δ_{47}, which may not be possible in high-resolution carbonate archives due to sample
593 size limitations. Analyzing small aliquots for combined $\delta^{18}O_c$ and Δ_{47} analyses consumes less material.
594 Secondly, individual summer and winter temperature reconstructions require large (> 1.5 mg; e.g.
595 Fernandez et al., 2017) Δ_{47} samples from seasonal extremes, which causes more time-averaging than the
596 approaches combining small aliquots. Finally, the position of seasonal extremes estimated from the $\delta^{18}O_c$
597 record may not reflect the true seasonal extent if seasonal SST and $\delta^{18}O_w$ cycles are not in phase (as in
598 case 9), causing the seasonal Δ_{47}-based SST reconstructions to underestimate the temperature
599 seasonality. In such cases, $\delta^{18}O_c$ and Δ_{47} analyses on small aliquots allow the seasonality in SST and $\delta^{18}O_w$
600 to be disentangled, yielding more accurate seasonality reconstructions.

601 Techniques for establishing independent age models for climate archives range from counting of growth
602 layers or increments (Schöne et al., 2008; Huyghe et al., 2019), modelling and extracting of rhythmic
603 variability in climate proxies through statistical approaches (e.g. De Ridder et al., 2007; Goodwin et al.,
604 2009; Judd et al., 2018; de Winter, 2021b) and interpolation of uncertainty on absolute dates (e.g. Scholz
605 and Hoffman, 2011; Meyers, 2019; Sinnesael et al., 2019). While propagating uncertainty in the data on
606 which age models are based onto the age model is relatively straightforward, errors on underlying *a priori*
607 assumptions such as linear growth rate between dated intervals, (quasi-)sinusoidal forcing of climate cycles
608 and the uncertainty on human-generated data such as layer counting are very difficult to quantify (e.g.
609 Comboul et al., 2014) and may not be normally distributed. Results of cases 25-29 show that uncertainties
610 in the age domain can significantly compromise reconstructions (**Fig. 12**). Within the scope of this study,
611 only the effect of symmetrical, normally distributed uncertainties on an artificial case with phase decoupled
612 SST and $\delta^{18}O_w$ seasonality (case 9) was tested. The effects of other types of uncertainties on the
613 reconstructions remain unknown, highlighting an unknown uncertainty in paleoseasonality and other high-
614 resolution paleoclimate studies that may introduce bias or lead to over-optimistic uncertainties on
615 reconstructions. Future research could quantify this unknown uncertainty by propagating estimates of
616 various types of uncertainty on depth values of samples and on the conversion from sampling to time
617 domain in age models.

618 **4.2 Conditions influencing success of reconstructions**

619 The reliability (accuracy and precision) of SST and $\delta^{18}O_w$ reconstructions depend on case-specific
620 conditions. The range of case studies tested in this study allowed us to evaluate the effect of variability in
621 SST, growth rate, $\delta^{18}O_w$, sampling resolution and record length relative to the control case (case 1; see
622 **S1**). A summary of the effects of these changes is given in **Table 2**.

623

Variable	cases	Metric	Effect on reconstructions			
			$\delta^{18}O$	smoothing	binning	optimization
SST	*12 15 17 19-21 30-33*	Precision	**0**	**+++**	**+**	**0**
		Accuracy	**+**	**+**	**0**	**+**
Growth rate	*2-6 14-18 30-33*	Precision	**+**	**++**	**++**	**+**
		Accuracy	**+**	**++**	**0**	**+**
$\delta^{18}O_w$	*7-11 13-18 30-33*	Precision	**+**	**++**	**0**	**0**
		Accuracy	**+++**	**+++**	**+**	**++**
Sampling resolution	*1-33*	Precision	**0**	**+++**	**++**	**++**
		Accuracy	**+**	**+**	**+++**	**+**
Record length	*22-24*	Precision	**0**	**0**	**+++**	**++**
		Accuracy	**+**	**0**	**++**	**++**
Age model uncertainty?	*25-29*	Precision	**+++**	**++**	**0**	**++**
		Accuracy	**+**	**+**	**++**	**++**

***Table 2**: Qualitative summary of the effects of changes in variables relative from the ideal case on reconstructions using the four approaches. The "cases" column lists cases in which the changes in the respective variable relative to the control case (case 1) were represented (see **Table 1** and **S1**). "0" = negligible effect, "+" = weak increase in uncertainty, "++" = moderate increase in uncertainty, "+++" = strong increase in uncertainty. Precision and accuracy of all tests is given in **S9**.*

4.2.1 SST variability

Variability in water temperature most directly affects the proxies under study. By default (case 1), SST varies sinusoidally around a MAT of 20°C with an amplitude of 10°C (see **2.3.3**, **Fig. 2** and **S1**). In cases in which multi-annual variability in SST is simulated (e.g. case 15 and 17), the accuracy of SST reconstructions using **$\delta^{18}O$** and **optimization** are reduced, while the **binning** approach is less strongly affected. Examples of such multi-annual cyclicity are El-Niño Southern Oscillation (ENSO; Philander, 1983) or North Atlantic Oscillation (NOA; Hurrell, 1995). The effect is especially large in case 17, which simulates a tropical environment with reduced SST seasonality and a strong multi-annual cyclicity. This type of environment is analogous to the environment of tropical shallow water corals, which are often used as archives for ENSO variability (e.g. Charles et al., 1997; Fairbanks et al., 1997) and is similar to tropical cases from the Australian Great Barrier Reef (case 31) and Red Sea (case 32; see **Fig. 3**). We therefore recommend using the **binning** approach on carbonate records where multi-annual cyclicity is prevalent and if a reliable age model can be established for these records (as in e.g. Sato, 1999; Scourse et al., 2006; Miyaji et al., 2010).

4.2.2 Growth rate variability and hiatuses

Figures 7 and 8 show that variations in the growth rate of records, including the occurrence of hiatuses, have a strong effect on reconstructions, especially using the **smoothing** approach. In general, hiatuses and slower growth reduce precision of monthly SST and $\delta^{18}O_w$ reconstructions by reducing mean temporal sampling resolution (samples/yr; see **Fig. 9**), and because parts of the record are undersampled. The effect on accuracy depends strongly on the timing of changes in growth rate or the occurrence of hiatuses. Cases 2-6 simulate specific growth rate effects and can be used to test these differences. The **smoothing** method is especially sensitive to changes in growth rate that take place in specific seasons, such as hiatuses in winter (case 2) or summer (case 3) and growth peaks in summer (case 5) or spring (case 6). The other reconstruction approaches are less affected by this bias, because they generally do not mix samples from different seasons. The **$\delta^{18}O$** method is especially well suited to deal with changes in growth rate because it does not require combining different aliquots for accurate SST reconstructions. The **binning** and **optimization** approaches are slightly less reliable in cases where growth rate decreases linearly or seasonally along the entire record (cases 4-6; **Fig. 2**). Because these two methods consider all samples in the records at once, they are more sensitive to changes in temporal sampling resolution along the record. It is worth noting that **optimization** is especially sensitive to sharp changes in growth rate in summer (e.g. cases 11, 14, 16 and 17) because those conditions force the **optimization** routine to use larger sample sizes or include samples outside the warmest month for summer temperature estimates. A potential solution to this problem could be to allow sample sizes of summer and winter groups to vary independently in the **optimization** routine (see 2.1). This would allow sample size in the undersampled season (in this case: summer) to become larger than that at the other end of the $\delta^{18}O_c$ spectrum, reducing uncertainty on the more densely sampled season and therefore improving the entire seasonality reconstruction.

A worst-case scenario is represented by case 18, where the cold half of the year is not recorded. Such cases result in strong biases in reconstructions of mean annual and seasonal ranges in SST and $\delta^{18}O_w$, regardless of which method is used. In such extreme cases the record simply contains insufficient information to reconstruct variability in growth rate, SST and $\delta^{18}O_w$, and it seems that no statistical method would enable this missing information to be recovered. The solution for these reconstructions would be to

establish reliable age models, independent of $\delta^{18}O$ or Δ_{47} data, which show that a large part of the seasonal cycle is missing. All methods used in this study rely on a conversion of SST and $\delta^{18}O_w$ reconstructions to the time domain to define monthly time bins. This conversion breaks down in fossil examples when the seasonal cycle cannot be extracted from the archive, which happens when half of the seasonal cycle or more is obscured by growth hiatuses, as exemplified in case 18.

While hiatuses encompassing half of the seasonal cycle are uncommon, changes in growth rate are common in accretionary carbonate archives because conditions for (biotic or abiotic) carbonate mineralization often vary over time. This variability is either driven by biological constraints, such as senescence (e.g. Schöne, 2008; Hendriks et al., 2012), the reproductive cycle (Gaspar et al., 1999) or stress (Surge et al., 2001; Compton et al., 2007) or by variations in the environment that promote or inhibit carbonate production, such as seasonal variations in temperature (Crossland, 1984; Bahr et al., 2017) or precipitation (Dayem et al., 2010; Van Rampelbergh et al., 2014). In general, such conditions occur more frequently in mid- to high-latitude environments than in low-latitudes, and in more coastal environments rather than in open marine settings, because these environments contain stronger variations in the factors that influence growth rates (e.g. temperature, precipitation or freshwater influx; e.g. Surge et al., 2001; Ullmann et al., 2010). This difference was simulated in the cases representing natural variability (case 14-18 and 30-33). Accuracy in the coastal high-latitude settings (cases 16, 18 and 29) are indeed more strongly affected by changes in growth rate. Because in such highly variable environments growth rate variability often co-occurs with variability in $\delta^{18}O_w$, using $\delta^{18}O_c$-based reconstructions is not advised, unless $\delta^{18}O_w$ variability can be constrained or neglected (which is rare in these environments).

Additional complications include that the lack of constraint on growth rate variability because of uncertainties in the record's age model (see **4.1.3**) and the effect of growth rate variability on the sampling resolution. The effect of growth rate on time-averaging within samples was not specifically tested in this study but introduces uncertainty in practice when archives with variable growth rate are sampled at a constant sampling resolution in the depth domain. In this case, parts of the archive with a lower growth rate yield more time-averaged samples, potentially dampening one extreme of the seasonal cycle (e.g. Goodwin et al., 2003). In highly dynamic environments it is challenging to isolate all variables that introduce bias, and

697 irregular variability in growth rate and $\delta^{18}O_w$ will invariably introduce uncertainty in SST reconstructions,
698 even when applying the best Δ_{47}-based approaches (e.g. **binning** and **optimization**). In such examples,
699 the results of natural variability cases (14-18 and 30-33) and of the real oyster data (**Fig. 6**) serve as
700 benchmarks for the degree of uncertainty that may remain unexplained in these records.

701 *4.2.3 Variability in* $\delta^{18}O_w$

702 As discussed in **4.1.1**, these variations in $\delta^{18}O_w$ have a large effect on the accuracy of $\delta^{18}O_c$-based
703 reconstructions, and their occurrence constitutes the main advantage of applying the Δ_{47} thermometer
704 (Eiler, 2011). However, results of cases 7-11 in **Fig. 8** and **Table 2** show that $\delta^{18}O_w$ variations can also bias
705 Δ_{47}-based reconstructions, especially those of seasonal ranges and using the **smoothing** approach.
706 **Smoothing** reconstructions are biased by these $\delta^{18}O_w$ shifts in much the same way as they are affected
707 by shifts in growth rate (see **4.2.2**). The **optimization** approach is sensitive to seasonal changes in $\delta^{18}O_w$
708 in antiphase with SST seasonality and by increases in $\delta^{18}O_w$ in summer (e.g. due to excess evaporation;
709 e.g. case 11), especially when used for reconstructions of $\delta^{18}O_w$ seasonality. This effect arises because
710 the **optimization** approach orders data based on $\delta^{18}O_c$ and Δ_{47} seasonality to isolate the $\delta^{18}O_w$-SST
711 relationship. Both antiphase $\delta^{18}O_w$ seasonality and summer evaporation dampen the seasonal $\delta^{18}O_c$ cycle
712 and therefore influences the reconstruction of the $\delta^{18}O_w$-SST relationship. A good example of this is seen
713 in the real oyster data (**Fig. 6**), where $\delta^{18}O_w$ and SST vary in phase and $\delta^{18}O_w$ dampens the SST
714 seasonality. The **binning** approach is more robust against $\delta^{18}O_w$ variability that dampens the seasonal
715 cycle and is therefore a better choice for absolute SST reconstructions in environments where summer
716 evaporation or other $\delta^{18}O_w$ variability in phase with SST seasonality is expected to occur, if the age model
717 is reliable enough to allow monthly binning of raw data (see **4.1.3**). Indeed, reconstructions from the
718 lagoonal environment (case 16) and Red Sea case (case 32 which is characterized by strong summer
719 evaporation; e.g. Titschack et al., 2010) show that **binning** is the most reliable choice in these
720 environments.

721 *4.2.4 Variability in sampling resolution and record length*

722 Other factors influencing the effectivity of reconstructions are the sampling resolution and the length of the
723 record. Many of the cases discussed in this study represent idealized cases with comparatively high

sampling resolutions over comparatively long (12 yr) paleoseasonality records, which yield large sample sizes. By comparison, the typical age of mollusks, which are often used as paleoseasonality archives, is 2-5 years (Ivany, 2012). Records with the highest sampling resolutions (0.1 and 0.2 mm) contain up to 1200 samples. Generating such records is not impossible, but it is highly unlikely to be applied in paleoclimate studies given the limitation of resources (e.g. instrument time) and the desire to analyze multiple records from different specimens, species, localities or ages to gain a better understanding of the variability in paleoseasonality (e.g. Goodwin et al., 2003; Schöne et al., 2006; Petersen et al., 2016). In some cases large datasets are meticulously collected from single carbonate records (e.g. Schöne et al., 2005; Vansteenberge et al., 2016; de Winter et al., 2020a; Shao et al., 2020). However, in such studies, the aim is often to investigate variability at a higher (e.g. daily; de Winter et al., 2020a) resolution or longer timescales (e.g. decadal to millennial; Schöne et al., 2005; Vansteenberge et al., 2016; Shao et al., 2020) in addition to the seasonal cycle, rather than to improve the reliability of reconstructing one type of variability (e.g. seasonality) alone.

Fig. 9 shows that increasing temporal sampling resolution (samples/yr) improves both the accuracy and precision of all Δ_{47}-based reconstructions. This occurs because Δ_{47} samples have a large analytical uncertainty (see **4.1.2**) and grouping of data therefore improves reconstructions. The decrease in precision of $\delta^{18}O_c$-based reconstructions (**Fig. 9C-D**) is explained by the fact that the analytical uncertainty of $\delta^{18}O_c$ measurements is much smaller than the variability introduced by natural sub-annual variability in SST and $\delta^{18}O_w$ unrelated to the seasonal cycle (see **S4**). Therefore, higher sampling resolutions allow $\delta^{18}O_c$ records to better capture this sub-seasonal variability, which introduces more noise on the seasonal cycle (reducing precision) but causes monthly mean SST and $\delta^{18}O_w$ to be more accurately reconstructed. Towards higher sampling resolutions, the gap in precision between $\delta^{18}O_c$- and Δ_{47}-based reconstructions closes, eventually (in an ideal case) diminishing the advantage of high analytical precision in $\delta^{18}O_c$ measurements (**Fig. 9C-D**).

An optimum sample resolution can be defined for each method after which improving sampling resolution does not significantly improve the reliability of the reconstruction (as in de Winter et al., 2017). **Figure 9** shows that this optimum varies depending on which variable (MAT, SST seasonality, mean annual $\delta^{18}O_w$

or $\delta^{18}O_w$ seasonality) is reconstructed. Therefore, **Fig. 9** will allow future researchers to determine the sampling resolution that is tailored to their purpose. In general, the improvement after a sample size of 20-30 samples per year is negligible for the **binning** and **optimization** methods if the total number of samples (depending on both sampling resolution and record length) is sufficient for monthly temperature reconstructions. Our data show that 200-250 paired $\delta^{18}O_c$ and Δ_{47} measurements are in general sufficient for a standard deviation of 2-3°C on monthly SST reconstructions using the **binning** or **optimization** approach (**Fig. 10**; **S5**).

Record length only has a minimal influence on the **optimization** method but for very short records (≤2 years) **binning** becomes very imprecise, especially at low sampling resolutions (**Fig. 11**). The reason is that the sample size within monthly time bins becomes too small in these cases, while the more flexible sample size window of the optimization routine circumvents this problem. The choice between these two approaches should therefore be based on a tradeoff between the length of the record (in time) and the number of samples that can be retrieved from it. As a result, shorter-lived, fast-growing climate archives, such as large or fast-growing (e.g. juvenile) mollusk shells, are best sampled using a high temporal resolution (>30 samples/yr) sampling strategy with the **optimization** approach. Longer lived archives with a lower mineralization rate, such as annually laminated speleothems, corals and gerontic mollusks, are best sampled using long time series at monthly resolution using the **binning** approach.

A simplified decision tree that could guide sampling strategies for future paleoseasonality studies is shown in **Figure 14**. Note that choices and tradeoffs for these reconstructions may differ depending on the archive and environment in which it formed (see discussion above).

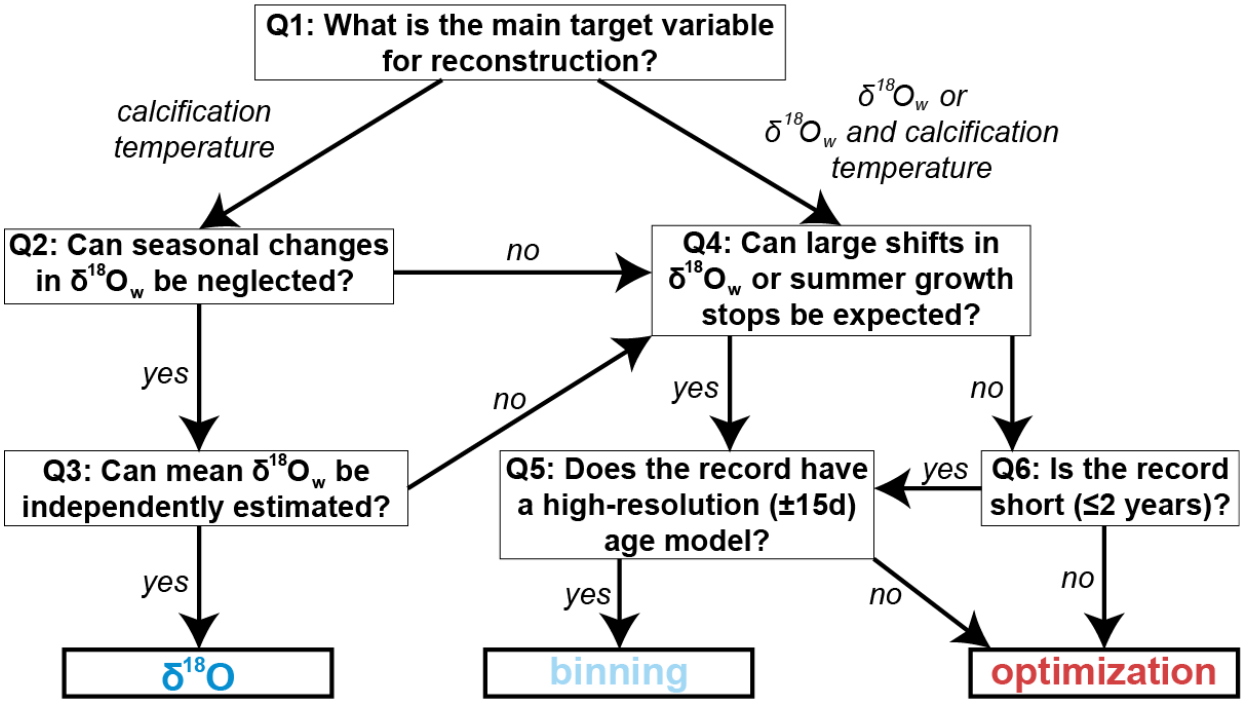

***Figure 15**: Schematic guide to choosing the right approach for reconstructing annual mean or seasonality in SST and $\delta^{18}O_w$ from accretionary carbonate archives. Recommendations are based on the results of testing all four approaches on the entire range of cases. Researchers can follow the six steps (questions Q1-6) to decide on the right approach for reconstructing the target variable. Guidelines are based on minimizing both accuracy and precision (see details in **S9**). Note that the **smoothing** approach is never the best choice. The choice between the two remaining Δ_{47}-based approaches (**binning** and **optimization**) relies heavily on the situation and may be driven by a preference for more accurate or more precise results.*

4.3 Implications for clumped isotope sample size

The **optimization** technique for grouping Δ_{47} aliquots for accurate SST and $\delta^{18}O_w$ reconstructions allows us to assess the limitations of the clumped isotope thermometer for temperature reconstructions from high-resolution carbonate archives. The optimal sample size given by the approach is different for different cases and depends on the temporal sampling resolution and the characteristics of the record (see **S4**). As expected, in cases more like the ideal case (case 1), optimal sample sizes are low (~14-24), while sample sizes increase in more complicated cases based on simulated natural environments (case 14-18) or cases based on actual SST and SSS data (cases 30-33). More confined SST seasonality (cases 19-21) also requires larger samples to reconstruct (up to 100 samples in some cases). This is not surprising, because

variability within samples will increase in records in which the seasonality is smaller or more obscured by other environmental variability. The optimal sample size between cases and sampling resolutions is not normally distributed but tails towards high sample sizes with some extreme outliers (Shapiro Wilk test $p << 0.05$; **S10**). The median sample size of all our simulations is 17 aliquots. This number lies between the minimum number of 14 ~100 µg replicates of standards calculated by Fernandez et al. (2017) and the minimum of 20-40 ~100 µg aliquots required for optimal paleoseasonality reconstruction from fossil bivalves by de Winter et al. (2020b). This is to be expected since many of the cases explored in this study represent ideal cases compared with the natural situation. However, in these virtual cases a measure of random sub-annual variability in SST and $\delta^{18}O_w$ was added (see **Fig. 4** and **S2**), simulating a more realistic environment and resulting in poorer precision than replicates of a carbonate standard (as in Fernandez et al., 2017). Our simulations show that the optimum number of samples to be combined in seasonality studies depends on both the analytical uncertainty of Δ_{47} measurements (as represented by the estimate in Fernandez et al., 2017) and the variability between aliquots pooled within a sample that is attributed to actual variability within the record (as represented by our simulations and the estimate in de Winter et al. 2020b). The optimal sample size is therefore a good measure for the limitations of temperature variability that can be resolved in a record and can help researchers decide which strategy to apply for combining measurements to obtain the most reliable paleoseasonality estimates, or to decide whether extra sampling is required, even if the chosen approach is not to use the **optimization** routine itself. Note that the optimum sample size is kept equal for summer and winter samples in this study, and that the **optimization** approach can likely achieve better performance by considering unequal sample sizes in opposite seasons (see 4.1.3 and 4.2.2). While this added flexibility comes at a higher computational cost due to the increased number of possible sample size combinations to be considered, future studies should investigate whether this updated **optimization** approach could yield more reliable seasonality reconstructions.

4.4 Implications for other sample size problems

While the discussion above focuses on optimizing approaches for combining samples for clumped isotope analyses in paleoseasonality reconstructions, the problem of combining samples to reduce uncertainty and isolate variation in datasets is very common (e.g. Zhang et al., 2004; Merz and Thieken,

2005; Tsukakoshi, 2011). Therefore, the approaches outlined and tested in this study have applications beyond paleoseasonality reconstructions. Examples of other problems that could benefit from applying similar approaches for reducing the uncertainty of estimates of target variables while minimizing the number of analyses required to meet analytical requirements include: (1) reconstructing paleoenvironmental variability in the terrestrial realm from tooth bioapatite (e.g. Passey and Cerling, 2002; Kohn, 2004; Van Dam and Reichart, 2009; de Winter et al., 2016), (2) quantitative time series analysis of orbital cycles in stratigraphic records (e.g. Lourens et al., 2010; de Vleeschouwer et al., 2017; Noorbergen et al., 2017; Westerhold et al., 2020), (3) strontium isotope dating (e.g McArthur et al., 2012; de Winter et al., 2020c), (4) reconstructing sub-seasonal variability from ultra-high-resolution records (e.g. from fast-growing mollusks and gastropods; e.g. Sano et al., 2012; Warter and Müller, 2017, de Winter et al., 2020d; Yan et al., 2020), and (5) reconstructing sea surface and deep-sea temperatures across short-lived (10–100 kyr) episodes of climate change or climate shifts from deep marine archives characterized by low sedimentation rates (e.g. Lear et al., 2008; Jenkyns, 2010; Stap et al., 2010; Lauretano et al., 2018). A more detailed discussion of the implications for other sample size problems is provided in the **Supplementary Information**.

5. Conclusions and recommendations

The performance of three Δ_{47}-based approaches to reconstruct seasonality from accretionary carbonate archives was evaluated in comparison with conventional $\delta^{18}O_c$-based reconstructions in a wide range of case studies. From the results, we conclude that while $\delta^{18}O_c$-based reconstructions (**$\delta^{18}O$**) yield superior precision for SST reconstructions, this method runs a high risk of yielding inaccurate results due to innate assumptions about the value of $\delta^{18}O_w$, which must be estimated and assumed constant year-round. Unless $\delta^{18}O_w$ can be independently constrained or variability in $\delta^{18}O_w$ can be neglected, Δ_{47}-based reconstructions should be the method of choice for absolute mean annual temperature and SST seasonality reconstructions. Various techniques for combining Δ_{47} data were evaluated. Our findings suggest that smoothing Δ_{47} data using a moving average almost allways cases in a dampening of the seasonal cycle which severely hampers recovery of seasonality. Applying the **smoothing** approach results in inaccuracies in reconstructions of MAT as well, especially in cases where part of the seasonal cycle is obscured by variability in growth rate or multi-annual trends. More reliable seasonality reconstructions are achieved with two approaches for combining Δ_{47} data using time binning (**binning**) or applying a flexible sample size optimization (**optimization**) approach. Of these two approaches, **optimization** achieves better precision and can resolve smaller seasonal temperature differences with confidence. However, **binning** is often more accurate, and outperforms **optimization** as the most reliable approach. This is especially true in cases with growth stops or $\delta^{18}O_w$ changes in phase with temperature seasonality (e.g. strong seasonal evaporation or freshwater influx) and in longer multi-annual time series with a reliable age model. **Optimization** is the better choice for shorter (<3 years) records, especially if the sampling resolution can be increased, such as in short, fast growing climate archives.

Despite the focus on the problem of resolving seasonality in carbonate archives, the findings in this study have applications for other problems in earth science where sample size and sampling resolution put limits on the ability to resolve specific trends, events, and cycles from time series. While the above-mentioned recommendations of the **optimization** and **binning** methods are likely valid for most studies aiming to quantify the mean and amplitude of a specific cycle or event (equivalent to MAT and SST seasonality),

(dynamic) moving averages (**smoothing**) are expected to yield the best results in studies quantifying aperiodic trends from longer data series.

Code availability

All scripts used to make the calculations described in this study are compiled in the documented R package "seasonalclumped", which is freely available on the open-source online R-database CRAN (de Winter, 2021a; https://cran.r-project.org/web/packages/seasonalclumped). Annotated R scripts used to make calculations for this study are available in the digital supplement uploaded to the open-source online repository Zenodo (www.doi.org/10.5281/zenodo.3899926).

Data availability

Supplementary data, figures and tables as well as all scripts used to do the calculations and create the virtual datasets used in this study are deposited in the open-source online repository Zenodo (www.doi.org/10.5281/zenodo.3899926). Virtual datasets generated within the context of this study are also made available as datafiles within the R package that contains the scripts used for this study ("seasonalclumped"; de Winter, 2021a; see https://cran.r-project.org/web/packages/seasonalclumped).

Author contributions

NJW designed the study, wrote the scripts for all calculations, and created a first draft of the manuscript text and figures. MZ, TA and NJW worked together from the first draft towards the final manuscript. All authors contributed to the representation of the data and methods in figures and to the discussion of the implications of the data in the discussion.

Competing Interests

The authors have no potential conflicts of interest to declare with regards to this study.

Acknowledgements

The authors would like to thank all members of the Clumped Isotope research group of Utrecht University, most notably Ilja Kocken and dr. Inigo Müller, for their comments and recommendations on a presentation of the initial results of this study.

Financial support

NJW is funded by the European Commission through a Marie Sklodowska Curie Individual Fellowship (UNBIAS, grant # 843011) and by the Flemish Research Council (FWO) through a Junior Postdoctoral Fellowship (12ZB220N).

References

Bahr, K. D., Jokiel, P. L. and Rodgers, K. S.: Seasonal and annual calcification rates of the Hawaiian reef coral, Montipora capitata, under present and future climate change scenarios, ICES J Mar Sci, 74(4), 1083–1091, https://doi.org/10.1093/icesjms/fsw078, 2017.

Bernasconi, S. M., Müller, I. A., Bergmann, K. D., Breitenbach, S. F., Fernandez, A., Hodell, D. A., Jaggi, M., Meckler, A. N., Millan, I. and Ziegler, M.: Reducing uncertainties in carbonate clumped isotope analysis through consistent carbonate-based standardization, Geochemistry, Geophysics, Geosystems, 19(9), 2895–2914, 2018.

Brand, W. A., Coplen, T. B., Vogl, J., Rosner, M. and Prohaska, T.: Assessment of international reference materials for isotope-ratio analysis (IUPAC Technical Report), Pure and Applied Chemistry, 86(3), 425–467, https://doi.org/10.1515/pac-2013-1023, 2014.

Briard, J., Pucéat, E., Vennin, E., Daëron, M., Chavagnac, V., Jaillet, R., Merle, D. and de Rafélis, M.: Seawater paleotemperature and paleosalinity evolution in neritic environments of the Mediterranean margin: Insights from isotope analysis of bivalve shells, Palaeogeography, Palaeoclimatology, Palaeoecology, 543, 109582, https://doi.org/10.1016/j.palaeo.2019.109582, 2020.

Caldarescu, D. E., Sadatzki, H., Andersson, C., Schäfer, P., Fortunato, H. and Meckler, A. N.: Clumped isotope thermometry in bivalve shells: A tool for reconstructing seasonal upwelling, Geochimica et Cosmochimica Acta, 294, 174–191, https://doi.org/10.1016/j.gca.2020.11.019, 2021.

Charles, C. D., Hunter, D. E. and Fairbanks, R. G.: Interaction between the ENSO and the Asian monsoon in a coral record of tropical climate, Science, 277(5328), 925–928, 1997.

Comboul, M., Emile-Geay, J., Evans, M. N., Mirnateghi, N., Cobb, K. M. and Thompson, D. M.: A probabilistic model of chronological errors in layer-counted climate proxies: applications to annually banded coral archives, Climate of the Past, 10(2), 825–841, 2014.

Compton, T. J., Rijkenberg, M. J. A., Drent, J. and Piersma, T.: Thermal tolerance ranges and climate variability: A comparison between bivalves from differing climates, Journal of Experimental Marine Biology and Ecology, 352(1), 200–211, https://doi.org/10.1016/j.jembe.2007.07.010, 2007.

Cook, E. R. and Kairiukstis, L. A.: Methods of dendrochronology: applications in the environmental sciences, Springer Science & Business Media., 2013.

Cramer, B. S., Toggweiler, J. R., Wright, J. D., Katz, M. E. and Miller, K. G.: Ocean overturning since the Late Cretaceous: Inferences from a new benthic foraminiferal isotope compilation, Paleoceanography, 24(4), https://doi.org/10.1029/2008PA001683, 2009.

Crossland, C.: Seasonal variations in the rates of calcification and productivity in the coral Acropora formosa on a high-latitude reef, Marine Ecology Progress Series, 15, 135–140, https://doi.org/10.3354/meps015135, 1984.

van Dam, J. A. and Reichart, G. J.: Oxygen and carbon isotope signatures in late Neogene horse teeth from Spain and application as temperature and seasonality proxies, Palaeogeography, Palaeoclimatology, Palaeoecology, 274(1–2), 64–81, https://doi.org/10.1016/j.palaeo.2008.12.022, 2009.

Dattalo, P.: Determining Sample Size: Balancing Power, Precision, and Practicality, Oxford University Press, USA., 2008.

Dayem, K. E., Molnar, P., Battisti, D. S. and Roe, G. H.: Lessons learned from oxygen isotopes in modern precipitation applied to interpretation of speleothem records of paleoclimate from eastern Asia, Earth and Planetary Science Letters, 295(1–2), 219–230, 2010.

De Ridder, F., de Brauwere, A., Pintelon, R., Schoukens, J., Dehairs, F., Baeyens, W. and Wilkinson, B. H.: Comment on: Paleoclimatic inference from stable isotope profiles of accretionary biogenic hardparts—a quantitative approach to the evaluation of incomplete data, by Wilkinson, B.H., Ivany, L.C., 2002. Palaeogeogr. Palaeocl. Palaeoecol. 185, 95–114, Palaeogeography, Palaeoclimatology, Palaeoecology, 248(3–4), 473–476, https://doi.org/10.1016/j.palaeo.2006.08.004, 2007.

De Vleeschouwer, D., Vahlenkamp, M., Crucifix, M. and Pälike, H.: Alternating Southern and Northern Hemisphere climate response to astronomical forcing during the past 35 my, Geology, 45(4), 375–378, 2017.

de Winter, N. J., Snoeck, C. and Claeys, P.: Seasonal Cyclicity in Trace Elements and Stable Isotopes of Modern Horse Enamel, PloS one, 11(11), e0166678, 2016.

de Winter, N., Sinnesael, M., Makarona, C., Vansteenberge, S. and Claeys, P.: Trace element analyses of carbonates using portable and micro-X-ray fluorescence: Performance and optimization of measurement parameters and strategies., Journal of Analytical Atomic Spectrometry, 32(6), 1211–1223, https://doi.org/10.1039/C6JA00361C, 2017.

de Winter, N. J., Vellekoop, J., Vorsselmans, R., Golreihan, A., Soete, J., Petersen, S. V., Meyer, K. W., Casadio, S., Speijer, R. P. and Claeys, P.: An assessment of latest Cretaceous Pycnodonte vesicularis (Lamarck, 1806) shells as records for palaeoseasonality: a multi-proxy investigation, Climate of the Past, 14(6), 725–749, 2018.

de Winter, N. J., Müller, I. A., Kocken, I. J., Thibault, N., Ullmann, C. V., Farnsworth, A., Lunt, D. J., Claeys, P. and Ziegler, M.: First absolute seasonal temperature estimates for greenhouse climate from clumped isotopes in bivalve shells, Nature Communications, in review, https://doi.org/10.21203/rs.3.rs-39203/v1, 2020a.

de Winter, N. J., Ullmann, C. V., Sørensen, A. M., Thibault, N., Goderis, S., Van Malderen, S. J. M., Snoeck, C., Goolaerts, S., Vanhaecke, F. and Claeys, P.: Shell chemistry of the boreal Campanian bivalve <i>Rastellum diluvianum</i> (Linnaeus, 1767) reveals temperature seasonality, growth rates and life cycle of an extinct Cretaceous oyster, Biogeosciences, 17(11), 2897–2922, https://doi.org/10.5194/bg-17-2897-2020, 2020b.

de Winter, N. J., Goderis, S., Malderen, S. J. M. V., Sinnesael, M., Vansteenberge, S., Snoeck, C., Belza, J., Vanhaecke, F. and Claeys, P.: Subdaily-Scale Chemical Variability in a Torreites Sanchezi Rudist Shell: Implications for Rudist Paleobiology and the Cretaceous Day-Night Cycle, Paleoceanography and Paleoclimatology, 35(2), e2019PA003723, https://doi.org/10.1029/2019PA003723, 2020c.

de Winter, N. J., Vellekoop, J., Clark, A. J., Stassen, P., Speijer, R. P. and Claeys, P.: The giant marine gastropod Campanile giganteum (Lamarck, 1804) as a high-resolution archive of seasonality in the Eocene greenhouse world, Geochemistry, Geophysics, Geosystems, 21(n/a), e2019GC008794, https://doi.org/10.1029/2019GC008794, 2020d.

de Winter, N. J.: seasonalclumped: Toolbox for Clumped Isotope Seasonality Reconstructions. https://CRAN.R-project.org/package=seasonalclumped, last access: 4 February 2021, 2021a.

de Winter, N. J.: ShellChron 0.2.8: A new tool for constructing chronologies in accretionary carbonate archives from stable oxygen isotope profiles, Geoscientific Model Development Discussions, 1–37, https://doi.org/10.5194/gmd-2020-401, 2021b.

Denton, G. H., Alley, R. B., Comer, G. C. and Broecker, W. S.: The role of seasonality in abrupt climate change, Quaternary Science Reviews, 24(10), 1159–1182, https://doi.org/10.1016/j.quascirev.2004.12.002, 2005.

Fairbanks, R. G., Evans, M. N., Rubenstone, J. L., Mortlock, R. A., Broad, K., Moore, M. D. and Charles, C. D.: Evaluating climate indices and their geochemical proxies measured in corals, Coral Reefs, 16(1), S93–S100, https://doi.org/10.1007/s003380050245, 1997.

Fernandez, A., Müller, I. A., Rodríguez-Sanz, L., van Dijk, J., Looser, N. and Bernasconi, S. M.: A reassessment of the precision of carbonate clumped isotope measurements: implications for calibrations and paleoclimate reconstructions, Geochemistry, Geophysics, Geosystems, 18(12), 4375–4386, 2017.

Gaspar, M. B., Ferreira, R. and Monteiro, C. C.: Growth and reproductive cycle of Donax trunculus L., (Mollusca: Bivalvia) off Faro, southern Portugal, Fisheries Research, 41(3), 309–316, https://doi.org/10.1016/S0165-7836(99)00017-X, 1999.

Goodwin, D. H., Schöne, B. R. and Dettman, D. L.: Resolution and fidelity of oxygen isotopes as paleotemperature proxies in bivalve mollusk shells: models and observations, Palaios, 18(2), 110–125, 2003.

992 Goodwin, D. H., Paul, P. and Wissink, C. L.: MoGroFunGen: A numerical model for reconstructing intra-
993 annual growth rates of bivalve molluscs, Palaeogeography, Palaeoclimatology, Palaeoecology, 276(1),
994 47–55, https://doi.org/10.1016/j.palaeo.2009.02.026, 2009.

995 Harwood, A. J. P., Dennis, P. F., Marca, A. D., Pilling, G. M. and Millner, R. S.: The oxygen isotope
996 composition of water masses within the North Sea, Estuarine, Coastal and Shelf Science, 78(2), 353–
997 359, https://doi.org/10.1016/j.ecss.2007.12.010, 2008.

998 Hendriks, I. E., Basso, L., Deudero, S., Cabanellas-Reboredo, M. and Álvarez, E.: Relative growth rates of
999 the noble pen shell Pinna nobilis throughout ontogeny around the Balearic Islands (Western
1000 Mediterranean, Spain), Journal of Shellfish Research, 31(3), 749–756, 2012.

1001 Henkes, G. A., Passey, B. H., Grossman, E. L., Shenton, B. J., Yancey, T. E. and Pérez-Huerta, A.:
1002 Temperature evolution and the oxygen isotope composition of Phanerozoic oceans from carbonate
1003 clumped isotope thermometry, Earth and Planetary Science Letters, 490, 40–50,
1004 https://doi.org/10.1016/j.epsl.2018.02.001, 2018.

1005 Hurrell, J. W.: Decadal trends in the North Atlantic Oscillation: regional temperatures and precipitation,
1006 Science, 269(5224), 676–679, 1995.

1007 Huybers, P. and Curry, W.: Links between annual, Milankovitch and continuum temperature variability,
1008 Nature, 441(7091), 329, 2006.

1009 Huyghe, D., Lartaud, F., Emmanuel, L., Merle, D. and Renard, M.: Palaeogene climate evolution in the
1010 Paris Basin from oxygen stable isotope (δ18O) compositions of marine molluscs, Journal of the
1011 Geological Society, 172(5), 576–587, 2015.

1012 Huyghe, D., de Rafélis, M., Ropert, M., Mouchi, V., Emmanuel, L., Renard, M. and Lartaud, F.: New insights
1013 into oyster high-resolution hinge growth patterns, Marine biology, 166(4), 48, 2019.

1014 IPCC: IPCC, 2013: Climate Change 2013: The Physical Science Basis. Contribution of Working Group I to
1015 the Fifth Assessment Report of the Intergovernmental Panel on Climate Change, 1535 pp, Cambridge
1016 Univ. Press, Cambridge, UK, and New York., 2013.

1017 Ivany, L. C.: Reconstructing paleoseasonality from accretionary skeletal carbonates—challenges and
1018 opportunities, The Paleontological Society Papers, 18, 133–166, 2012.

1019 Jenkyns, H. C.: Geochemistry of oceanic anoxic events, Geochemistry, Geophysics, Geosystems, 11(3),
1020 https://doi.org/10.1029/2009GC002788, 2010.

1021 Jones, A. M., Iacumin, P. and Young, E. D.: High-resolution d18O analysis of tooth enamel phosphate by
1022 isotope ratio monitoring gas chromatography mass spectrometry and ultraviolet laser fluorination, , 8,
1023 1999.

1024 Judd, E. J., Wilkinson, B. H. and Ivany, L. C.: The life and time of clams: Derivation of intra-annual growth
1025 rates from high-resolution oxygen isotope profiles, Palaeogeography, Palaeoclimatology, Palaeoecology,
1026 490, 70–83, 2018.

1027 Keating-Bitonti, C. R., Ivany, L. C., Affek, H. P., Douglas, P. and Samson, S. D.: Warm, not super-hot,
1028 temperatures in the early Eocene subtropics, Geology, 39(8), 771–774,
1029 https://doi.org/10.1130/G32054.1, 2011.

1030 Kele, S., Breitenbach, S. F., Capezzuoli, E., Meckler, A. N., Ziegler, M., Millan, I. M., Kluge, T., Deák, J.,
1031 Hanselmann, K. and John, C. M.: Temperature dependence of oxygen-and clumped isotope fractionation
1032 in carbonates: a study of travertines and tufas in the 6–95 C temperature range, Geochimica et
1033 Cosmochimica Acta, 168, 172–192, 2015.

1034 Kim, S.-T. and O'Neil, J. R.: Equilibrium and nonequilibrium oxygen isotope effects in synthetic carbonates,
1035 Geochimica et Cosmochimica Acta, 61(16), 3461–3475, https://doi.org/10.1016/S0016-7037(97)00169-
1036 5, 1997.

1037 Kocken, I. J., Müller, I. A. and Ziegler, M.: Optimizing the Use of Carbonate Standards to Minimize
1038 Uncertainties in Clumped Isotope Data, Geochemistry, Geophysics, Geosystems, 20(11), 5565–5577,
1039 https://doi.org/10.1029/2019GC008545, 2019.

1040 Kohn, M. J.: Comment: tooth enamel mineralization in ungulates: implications for recovering a primary
1041 isotopic time-series, by BH Passey and TE Cerling (2002), Geochimica et Cosmochimica Acta, 68(2),
1042 403–405, 2004.

1043 Lauretano, V., Zachos, J. C. and Lourens, L. J.: Orbitally Paced Carbon and Deep-Sea Temperature
1044 Changes at the Peak of the Early Eocene Climatic Optimum, Paleoceanography and Paleoclimatology,
1045 33(10), 1050–1065, https://doi.org/10.1029/2018PA003422, 2018.

1046 Lear, C. H., Bailey, T. R., Pearson, P. N., Coxall, H. K. and Rosenthal, Y.: Cooling and ice growth across
1047 the Eocene-Oligocene transition, Geology, 36(3), 251–254, 2008.

1048 LeGrande, A. N. and Schmidt, G. A.: Global gridded data set of the oxygen isotopic composition in
1049 seawater, Geophysical research letters, 33(12), 2006.

1050 Lisiecki, L. E. and Raymo, M. E.: A Pliocene-Pleistocene stack of 57 globally distributed benthic δ18O
1051 records, Paleoceanography, 20(1), https://doi.org/10.1029/2004PA001071, 2005.

1052 Lourens, L. J., Sluijs, A., Kroon, D., Zachos, J. C., Thomas, E., Röhl, U., Bowles, J. and Raffi, I.:
1053 Astronomical pacing of late Palaeocene to early Eocene global warming events, Nature, 435(7045),
1054 1083–1087, https://doi.org/10.1038/nature03814, 2005.

1055 Lourens, L. J., Becker, J., Bintanja, R., Hilgen, F. J., Tuenter, E., Van de Wal, R. S. and Ziegler, M.: Linear
1056 and non-linear response of late Neogene glacial cycles to obliquity forcing and implications for the
1057 Milankovitch theory, Quaternary Science Reviews, 29(1–2), 352–365, 2010.

1058 McArthur, J. M., Howarth, R. J. and Shields, G. A.: Strontium isotope stratigraphy, The geologic time scale,
1059 1, 127–144, 2012.

1060 Meckler, A. N., Ziegler, M., Millán, M. I., Breitenbach, S. F. and Bernasconi, S. M.: Long-term performance
1061 of the Kiel carbonate device with a new correction scheme for clumped isotope measurements, Rapid
1062 Communications in Mass Spectrometry, 28(15), 1705–1715, 2014.

1063 Merz, B. and Thieken, A. H.: Separating natural and epistemic uncertainty in flood frequency analysis,
1064 Journal of Hydrology, 309(1–4), 114–132, 2005.

1065 Meyers, S. R.: Astrochron: An R package for astrochronology, http://cran.r-
1066 project.org/package=astrochron.
1067 http://scholar.google.com/scholar?cluster=14876361610707754388&hl=en&oi=scholarr, last access: 30
1068 May 2017, 2014.

1069 Meyers, S. R.: Cyclostratigraphy and the problem of astrochronologic testing, Earth-Science Reviews, 190,
1070 190–223, https://doi.org/10.1016/j.earscirev.2018.11.015, 2019.

1071 Miyaji, T., Tanabe, K., Matsushima, Y., Sato, S., Yokoyama, Y. and Matsuzaki, H.: Response of daily and
1072 annual shell growth patterns of the intertidal bivalve Phacosoma japonicum to Holocene coastal climate
1073 change in Japan, Palaeogeography, Palaeoclimatology, Palaeoecology, 286(3), 107–120,
1074 https://doi.org/10.1016/j.palaeo.2009.11.032, 2010.

1075 Mook, W. G.: Stable carbon and oxygen isotopes of natural waters in the Netherlands, Isotope hydrology,
1076 1970, 163–190, 1970.

1077 Morgan, V. and van Ommen, T. D.: Seasonality in late-Holocene climate from ice-core records, The
1078 Holocene, 7(3), 351–354, https://doi.org/10.1177/095968369700700312, 1997.

1079 Mosley-Thompson, E., Thompson, L. G., Dai, J., Davis, M. and Lin, P. N.: Climate of the last 500 years:
1080 High resolution ice core records, Quaternary Science Reviews, 12(6), 419–430,
1081 https://doi.org/10.1016/S0277-3791(05)80006-X, 1993.

1082 Müller, I. A., Fernandez, A., Radke, J., van Dijk, J., Bowen, D., Schwieters, J. and Bernasconi, S. M.:
1083 Carbonate clumped isotope analyses with the long-integration dual-inlet (LIDI) workflow: scratching at
1084 the lower sample weight boundaries: LIDI as key for more precise analyses on much less carbonate
1085 material, Rapid Communications in Mass Spectrometry, 31(12), 1057–1066,
1086 https://doi.org/10.1002/rcm.7878, 2017.

1087 Noorbergen, L. J., Abels, H. A., Hilgen, F. J., Robson, B. E., Jong, E. de, Dekkers, M. J., Krijgsman, W.,
1088 Smit, J., Collinson, M. E. and Kuiper, K. F.: Conceptual models for short-eccentricity-scale climate control
1089 on peat formation in a lower Palaeocene fluvial system, north-eastern Montana (USA), Sedimentology,
1090 65(3), 775–808, https://doi.org/10.1111/sed.12405, 2018.

1091 O'Donnell, M. S. and Ignizio, D. A.: Bioclimatic predictors for supporting ecological applications in the
1092 conterminous United States, US Geological Survey Data Series, 691(10), 2012.

1093 Passey, B. H. and Cerling, T. E.: Tooth enamel mineralization in ungulates: implications for recovering a
1094 primary isotopic time-series, Geochimica et Cosmochimica Acta, 66(18), 3225–3234, 2002.

1095 Petersen, S. V., Tabor, C. R., Lohmann, K. C., Poulsen, C. J., Meyer, K. W., Carpenter, S. J., Erickson, J.
1096 M., Matsunaga, K. K., Smith, S. Y. and Sheldon, N. D.: Temperature and salinity of the Late Cretaceous
1097 western interior seaway, Geology, 44(11), 903–906, 2016.

1098 Philander, S. G. H.: El Nino southern oscillation phenomena, Nature, 302(5906), 295–301, 1983.

1099 R Core Team: R: A language and environment for statistical computing. R Foundation for Statistical
1100 Computing, Vienna, Austria. http://www.R-project.org/, 2013.

1101 Rodríguez-Sanz, L., Bernasconi, S. M., Marino, G., Heslop, D., Müller, I. A., Fernandez, A., Grant, K. M.
1102 and Rohling, E. J.: Penultimate deglacial warming across the Mediterranean Sea revealed by clumped
1103 isotopes in foraminifera, Scientific Reports, 7(1), 1–11, https://doi.org/10.1038/s41598-017-16528-6,
1104 2017.

1105 Rohling, E. J.: Oxygen isotope composition of seawater, The Encyclopedia of Quaternary Science.
1106 Amsterdam: Elsevier, 2, 915–922, 2013.

Sano, Y., Kobayashi, S., Shirai, K., Takahata, N., Matsumoto, K., Watanabe, T., Sowa, K. and Iwai, K.: Past daily light cycle recorded in the strontium/calcium ratios of giant clam shells, Nature Communications, 3, 761, 2012.

Sato, S.: Temporal change of life-history traits in fossil bivalves: an example of Phacosoma japonicum from the Pleistocene of Japan, Palaeogeography, Palaeoclimatology, Palaeoecology, 154(4), 313–323, https://doi.org/10.1016/S0031-0182(99)00106-6, 1999.

Schmitt, J., Schneider, R., Elsig, J., Leuenberger, D., Lourantou, A., Chappellaz, J., Kohler, P., Joos, F., Stocker, T. F., Leuenberger, M. and Fischer, H.: Carbon Isotope Constraints on the Deglacial CO2 Rise from Ice Cores, Science, 336(6082), 711–714, https://doi.org/10.1126/science.1217161, 2012.

Scholz, D. and Hoffmann, D. L.: StalAge–An algorithm designed for construction of speleothem age models, Quaternary Geochronology, 6(3–4), 369–382, 2011.

Schöne, B. R.: The curse of physiology—challenges and opportunities in the interpretation of geochemical data from mollusk shells, Geo-Marine Letters, 28(5–6), 269–285, 2008.

Schöne, B. R., Fiebig, J., Pfeiffer, M., Gleß, R., Hickson, J., Johnson, A. L., Dreyer, W. and Oschmann, W.: Climate records from a bivalved Methuselah (Arctica islandica, Mollusca; Iceland), Palaeogeography, Palaeoclimatology, Palaeoecology, 228(1–2), 130–148, 2005.

Schöne, B. R., Rodland, D. L., Fiebig, J., Oschmann, W., Goodwin, D., Flessa, K. W. and Dettman, D.: Reliability of multitaxon, multiproxy reconstructions of environmental conditions from accretionary biogenic skeletons, The Journal of geology, 114(3), 267–285, 2006.

Scourse, J., Richardson, C., Forsythe, G., Harris, I., Heinemeier, J., Fraser, N., Briffa, K. and Jones, P.: First cross-matched floating chronology from the marine fossil record: data from growth lines of the long-lived bivalve mollusc Arctica islandica, The Holocene, 16(7), 967–974, https://doi.org/10.1177/0959683606hl987rp, 2006.

Sha, L., Mahata, S., Duan, P., Luz, B., Zhang, P., Baker, J., Zong, B., Ning, Y., Brahim, Y. A., Zhang, H., Edwards, R. L. and Cheng, H.: A novel application of triple oxygen isotope ratios of speleothems, Geochimica et Cosmochimica Acta, 270, 360–378, https://doi.org/10.1016/j.gca.2019.12.003, 2020.

Shao, D., Mei, Y., Yang, Z., Wang, Y., Yang, W., Gao, Y., Yang, L. and Sun, L.: Holocene ENSO variability in the South China Sea recorded by high-resolution oxygen isotope records from the shells of Tridacna spp., Scientific Reports, 10(1), 3921, https://doi.org/10.1038/s41598-020-61013-2, 2020.

Sinnesael, M., De Vleeschouwer, D., Zeeden, C., Batenburg, S. J., Da Silva, A.-C., de Winter, N. J., Dinarès-Turell, J., Drury, A. J., Gambacorta, G. and Hilgen, F. J.: The Cyclostratigraphy Intercomparison Project (CIP): consistency, merits and pitfalls, Earth-Science Reviews, 102965, 2019.

Stap, L., Lourens, L. J., Thomas, E., Sluijs, A., Bohaty, S. and Zachos, J. C.: High-resolution deep-sea carbon and oxygen isotope records of Eocene Thermal Maximum 2 and H2, Geology, 38(7), 607–610, 2010.

Steffensen, J. P., Andersen, K. K., Bigler, M., Clausen, H. B., Dahl-Jensen, D., Fischer, H., Goto-Azuma, K., Hansson, M., Johnsen, S. J. and Jouzel, J.: High-resolution Greenland ice core data show abrupt climate change happens in few years, Science, 321(5889), 680–684, 2008.

Steuber, T., Rauch, M., Masse, J.-P., Graaf, J. and Malkoč, M.: Low-latitude seasonality of Cretaceous temperatures in warm and cold episodes, Nature, 437(7063), 1341–1344, https://doi.org/10.1038/nature04096, 2005.

Surge, D., Lohmann, K. C. and Dettman, D. L.: Controls on isotopic chemistry of the American oyster, Crassostrea virginica: implications for growth patterns, Palaeogeography, Palaeoclimatology, Palaeoecology, 172(3), 283–296, 2001.

Titschack, J., Zuschin, M., Spötl, C. and Baal, C.: The giant oyster Hyotissa hyotis from the northern Red Sea as a decadal-scale archive for seasonal environmental fluctuations in coral reef habitats, Coral Reefs, 29(4), 1061–1075, 2010.

Treble, P., Shelley, J. M. G. and Chappell, J.: Comparison of high resolution sub-annual records of trace elements in a modern (1911–1992) speleothem with instrumental climate data from southwest Australia, Earth and Planetary Science Letters, 216(1), 141–153, https://doi.org/10.1016/S0012-821X(03)00504-1, 2003.

Tsukakoshi, Y.: Sampling variability and uncertainty in total diet studies, Analyst, 136(3), 533–539, https://doi.org/10.1039/C0AN00397B, 2011.

Tudhope, A. W.: Variability in the El Nino-Southern Oscillation Through a Glacial-Interglacial Cycle, Science, 291(5508), 1511–1517, https://doi.org/10.1126/science.1057969, 2001.

Ullmann, C. V., Wiechert, U. and Korte, C.: Oxygen isotope fluctuations in a modern North Sea oyster (Crassostrea gigas) compared with annual variations in seawater temperature: Implications for palaeoclimate studies, Chemical Geology, 277(1), 160–166, 2010.

Van Rampelbergh, M., Verheyden, S., Allan, M., Quinif, Y., Keppens, E. and Claeys, P.: Seasonal variations recorded in cave monitoring results and a 10 year monthly resolved speleothem δ18O and δ13C record from the Han-sur-Lesse cave, Belgium, Climate of the Past Discussions, 10, 1821–1856, 2014.

Vansteenberge, S., Verheyden, S., Cheng, H., Edwards, R. L., Keppens, E. and Claeys, P.: Paleoclimate in continental northwestern Europe during the Eemian and early Weichselian (125–97 ka): insights from a Belgian speleothem, Clim. Past, 12(7), 1445–1458, https://doi.org/10.5194/cp-12-1445-2016, 2016.

Vansteenberge, S., Winter, N. de, Sinnesael, M., Verheyden, S., Goderis, S., Malderen, S. J. M. V., Vanhaecke, F. and Claeys, P.: Reconstructing seasonality through stable isotope and trace element analysis of the Proserpine stalagmite, Han-sur-Lesse Cave, Belgium: indications for climate-driven changes during the last 400 years, Climate of the Past Discussions, 1–32, https://doi.org/10.5194/cp-2019-78, 2019.

Veizer, J. and Prokoph, A.: Temperatures and oxygen isotopic composition of Phanerozoic oceans, Earth-Science Reviews, 146, 92–104, https://doi.org/10.1016/j.earscirev.2015.03.008, 2015.

Vleeschouwer, D. D., Vahlenkamp, M., Crucifix, M. and Pälike, H.: Alternating Southern and Northern Hemisphere climate response to astronomical forcing during the past 35 m.y., Geology, 45(4), 375–378, https://doi.org/10.1130/G38663.1, 2017.

Warter, V. and Müller, W.: Daily growth and tidal rhythms in Miocene and modern giant clams revealed via ultra-high resolution LA-ICPMS analysis—A novel methodological approach towards improved sclerochemistry, Palaeogeography, Palaeoclimatology, Palaeoecology, 465, 362–375, 2017.

1184 Westerhold, T., Marwan, N., Drury, A. J., Liebrand, D., Agnini, C., Anagnostou, E., Barnet, J. S., Bohaty,
1185 S. M., De Vleeschouwer, D. and Florindo, F.: An astronomically dated record of Earth's climate and its
1186 predictability over the last 66 million years, Science, 369(6509), 1383–1387, 2020.

1187 Wilkinson, B. H. and Ivany, L. C.: Paleoclimatic inference from stable isotope profiles of accretionary
1188 biogenic hardparts – a quantitative approach to the evaluation of incomplete data, Palaeogeography,
1189 Palaeoclimatology, Palaeoecology, 185(1), 95–114, https://doi.org/10.1016/S0031-0182(02)00279-1,
1190 2002.

1191 Yan, H., Liu, C., An, Z., Yang, W., Yang, Y., Huang, P., Qiu, S., Zhou, P., Zhao, N. and Fei, H.: Extreme
1192 weather events recorded by daily to hourly resolution biogeochemical proxies of marine giant clam shells,
1193 Proceedings of the National Academy of Sciences, 2020.